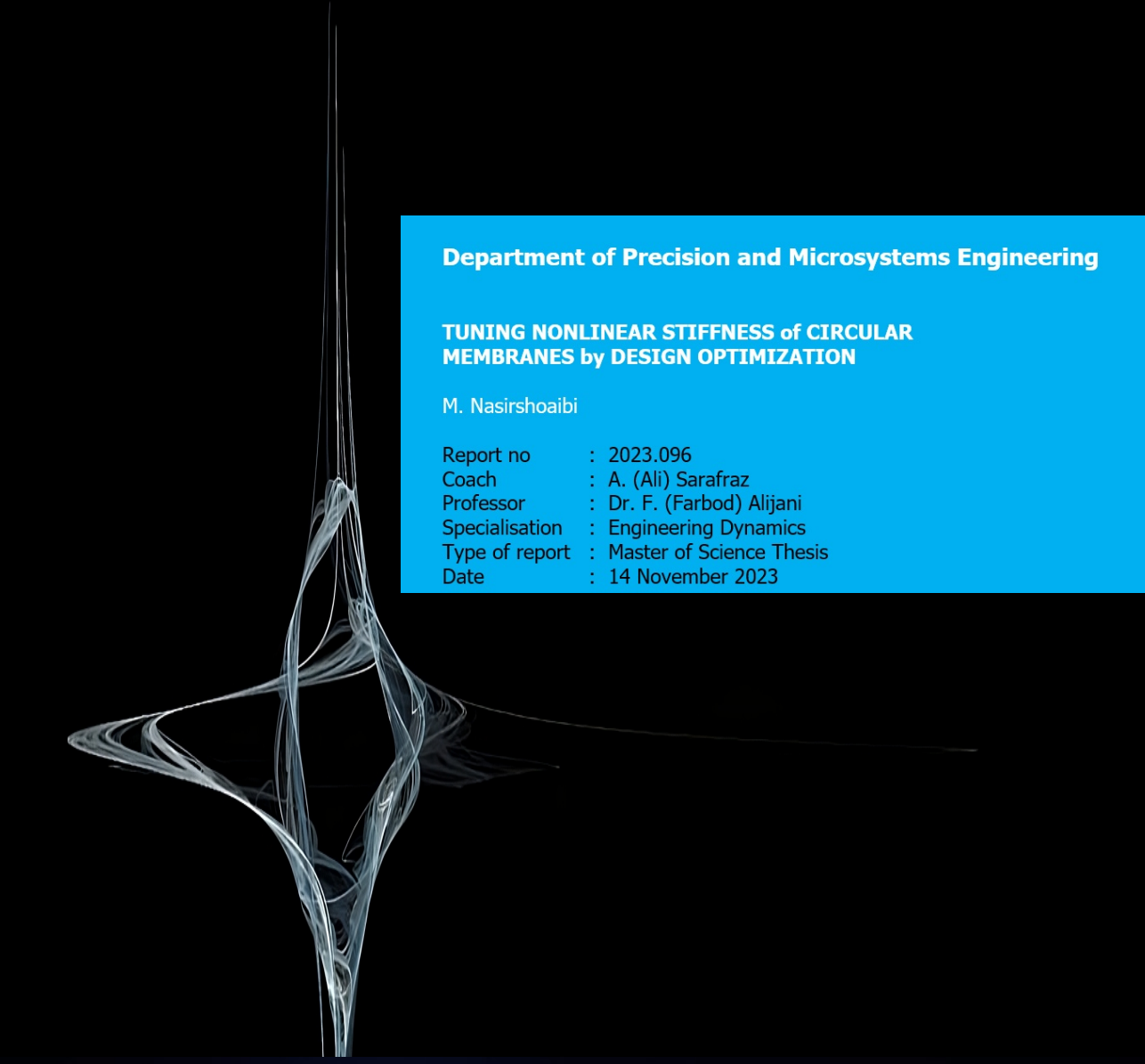

Department of Precision and Microsystems Engineering

TUNING NONLINEAR STIFFNESS of CIRCULAR MEMBRANES by DESIGN OPTIMIZATION

M. Nasirshoaibi

Report no : 2023.096
Coach : A. (Ali) Sarafraz
Professor : Dr. F. (Farbod) Alijani
Specialisation : Engineering Dynamics
Type of report : Master of Science Thesis
Date : 14 November 2023

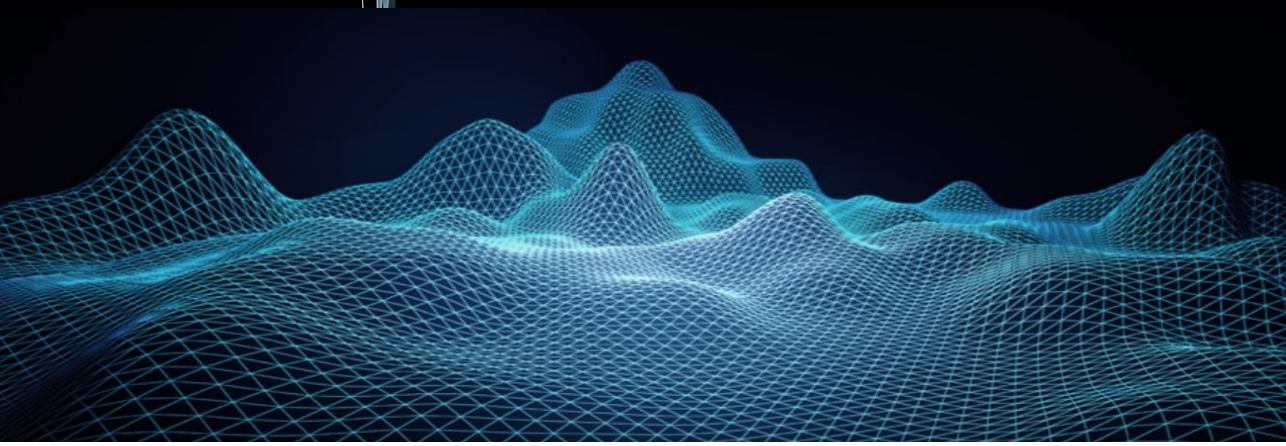

TU Delft Delft University of Technology

Challenge the future

TUNING NONLINEAR STIFFNESS OF CIRCULAR MEMBRANES BY DESIGN OPTIMIZATION

Master of Science Thesis

For the degree of Master of Science in Mechanical Engineering at Delft University of Technology

by

Mehrdad NASIRSHOAIBI
Student number: 5620252
November 2023
Professor: Dr. F. (Farbod) Alijani
Weekly Coach: A. (Ali) Sarafraz
Thesis Defense Date: November 22, 2023 at 13:00 PM

Dynamics of Micro and Nanosystems
Faculty of Mechanical, Maritime and Materials Engineering (3mE)
Delft University of Technology

TU Delft Delft University of Technology

If I'm going to fall, I don't want to fall back on anything except my faith. I want to fall forward. I figure at least this way, I'll see what I'm going to hit.

Denzel Washington

PREFACE

IN the realm of micro- and nano-mechanics, a world unfolds where minuscule entities wield substantial influence. This innovative field of mechanics intricately explores the behaviors of materials and devices at micro- and nano-scales. Within this thesis, a journey commences through the realms of micro- and nano-mechanics, aiming to unveil novel insights into the enthralling domain of nonlinear dynamics. The study of this field is both exciting and promising, offering boundless opportunities to unravel previously unknown mechanical properties and phenomena that hold the potential to revolutionize the methodologies of design and creation.

This thesis aims to explore various questions, delving into the complexities of nonlinear dynamics and endeavoring to unearth answers that might lead to new discoveries. As you delve into this thesis, I hope that you, the reader, will find yourself captivated by the enthralling world of nonlinear dynamics, much like I have been throughout this research endeavor. I firmly believe that the concepts and principles articulated in this thesis bear the potential to propel our comprehension of nonlinear dynamics forward, and I am enthusiastic about sharing this journey with you.

Mehrdad Nasirshoaibi
Delft, November 2023

ACKNOWLEDGEMENTS

I would like to express my heartfelt gratitude to all those who have played a significant role in the completion of my master's thesis. The journey to complete my thesis was not without its challenges, including time constraints and research hurdles, both personal and academic. Nevertheless, I always held onto the belief that there would be something positive waiting for me at the end. This thesis has been a tremendous learning experience, teaching me the value of perseverance and determination in both my academic and personal lives.

I am deeply grateful to my professor, Dr. F. (Farbod) Alijani, for his unwavering support, vast knowledge, and unwavering guidance throughout the project. I also extend my heartfelt appreciation to my weekly coach, A. (Ali) Sarafraz, for his pleasant company during my thesis and continuous supervision, which significantly contributed to achieving improved results and a better understanding of the work.

My appreciation extends to the valuable assistance provided by Z. (Zichao) Li and V. (Vincent) Bos during my project, both of whom played instrumental roles in the successful completion of this work.

My deepest gratitude goes to my parents, brother, family, and friends, who have been my pillars of support. Their unwavering encouragement and belief in me were the driving force behind my perseverance in this challenging journey.

Finally, I would like to seize this opportunity to express my gratitude to all my lecturers and professors for their guidance and knowledge, which ignited my passion for the field of science and laid the foundation for this research. In conclusion, it is through the collective support of my academic mentors, friends, and family that I stand here today, having learned valuable life lessons and academic skills during this profound journey.

Mehrdad Nasirshoaibi
Delft, November 2023

CONTENTS

1

INTRODUCTION

OVER the last three decades, the field of micro- and nano-scale systems and technology has undergone substantial growth, drawing increased attention due to its potential applications and the observation of novel physical phenomena at this small scale.

Researchers have dedicated their efforts to the synthesis of materials and the development of microscopic and nanoscopic devices, unveiling a range of mechanical features that challenge conventional understanding. The discovery of these extraordinary mechanical features has sparked the curiosity of researchers, driving them to explore new frontiers in the field of micro- and nano-mechanics. These novel features necessitate more profound explorations through a combination of experimental and theoretical investigations.

In the realm of micro- and nano-scale experiments, advancing in experimental mechanics poses a substantial challenge in comparison to theoretical analyses and numerical simulations. This challenge arises since these small-scale experiments require not only a profound understanding of measurement principles and concepts but also the application of advanced measurement techniques and testing platforms.

Thinness results in very low bending rigidity, requiring only minimal energy for bending. This means that a small amount of mass or pressure can easily deform the device since it doesn't require much energy. It can also undergo significant bending with ease, and when subjected to large deformations, the device enters a nonlinear regime.

The inherent nonlinearity in the dynamics of micro- and nano-scale systems can significantly impact device performance and functionality. It can be both advantageous and challenging. Understanding and controlling nonlinear dynamics are essential for optimizing micro- and nano-scale devices, maximizing benefits while minimizing drawbacks

While nonlinear phenomena in mechanical systems are well understood, strategies for systematically designing structures with nonlinear responses have received little attention. Researchers are continually working to develop innovative techniques for modeling and optimizing these systems, paving the way for their expanded utility in a wide range of fields. In recent years, there has been a growing interest in using optimization tech-

niques to fine-tune the linear and nonlinear dynamics of small-scale systems [1]. These techniques involves the optimization of a system's parameters to achieve a desired nonlinear response.

Design optimization is a systematic and iterative process aimed to improve the performance and efficiency of a system. It involves exploring various design choices and parameters to find the best possible solution that meets specific criteria or objectives, such as maximizing performance. This process often employs mathematical models, simulations, and algorithms to analyze and refine designs. The use of design optimization techniques for tuning nonlinear dynamics has important implications for the development of micro- and nano-scale devices, such as sensors, actuators, and signal processors [2]. By optimizing the nonlinear response of these devices, it is possible to achieve enhanced performance, improved energy efficiency, and better control over their behavior.

To reduce the computational burden associated with high-dimensional problems and make it more feasible to analyze, control, or optimize large-scale systems in real-time or with limited computational resources, Reduced Order Models (ROMs) can be employed. ROMs are powerful computational techniques utilized in various fields to simplify complex systems and simulations while retaining essential information. They achieve this by reducing the dimensionality of the problem space and the governing equations of motion.

In the design optimization process for real-world problems, the number of design variables can often be substantial. To effectively address these complex and high-dimensional optimization tasks, the use of advanced algorithms is crucial. Modern techniques such as Stochastic algorithms have emerged as valuable tools in this context. Their ability to navigate complex, high-dimensional search spaces has made them a popular choice for tackling real-world optimization challenges with numerous design variables.

In this thesis, a novel methodology has been devised that empowers the optimization of the nonlinear vibration characteristics of devices featuring intricate geometries. The innovation extends to the development of a versatile routine capable of defining complex geometries and facilitating design within a Finite Element Method (FEM) framework. This routine operates in tandem with optimization algorithms, enabling us to identify and refine the most optimal designs. This approach not only streamlines the process but also offers the flexibility needed to tackle complex geometrical configurations, making it a powerful tool for enhancing the performance and efficiency of devices subjected to nonlinear vibrations.

To address a specific problem, a design challenge is introduced, involving a clamped circular membrane (drum). Circular voids of various radii and positions are incorporated within this membrane. The goal is to discover the arrangement that optimizes the nonlinear stiffness, whether it involves maximizing or minimizing it. The critical design parameters under consideration include the positions and radii of these circular voids. Additionally, specific constraints within the problem are established and defined to guide design choices.

Within this thesis, my approach involves the application of the Stiffness Evaluation Procedure (STEP) method as a Reduced Order Model (ROM) for constructing a nonlinear reduced-order model. This technique allows us to effectively reduce an infinite number of degrees of freedom (DOF) down to a single DOF, making complex systems more manageable. A parametric study is conducted to enhance the understanding of how the nonlinear stiffness of a circular membrane is influenced by the addition of circular voids with varying radii and positions. The Particle Swarm Optimization (PSO) algorithm is utilized for optimizing the design, enabling the control and fine-tuning of design parameters to identify the most optimal configuration. This integrated approach enables a streamlined process for achieving the best possible design, even in scenarios involving intricate and nonlinear systems with numerous degrees of freedom.

The central focus of this thesis is to introduce particle swarm optimization as an innovative methodology for nonlinear dynamic design optimization, with the goal of achieving precise identification of the optimal design. This research is guided by two primary objectives: the first is to assess the impact of introducing circular voids on the nonlinear stiffness of circular membranes, and the second is to pinpoint the optimal design with accuracy by utilizing particle swarm optimization.

1.1. RESEARCH QUESTIONS

This thesis is mainly focused on the following research questions:

- How does the presence of voids in circular membranes impact their nonlinear stiffness characteristics?
- How can design optimization techniques efficiently enhance the nonlinear dynamics and performance of dynamic systems?

1.2. THESIS OUTLINE

This study takes a systematic approach to investigate the research problems outlined earlier. The following sections delve into the research process, offering a comprehensive exploration and structure of our inquiry.

This thesis is organized into five main chapters. Chapter 1 serves as the introduction, offering insights into the subject's motivation and the research questions. In Chapter 2, the focus shifts to the literature review, covering nonlinearity and its sources, current research on nonlinearity tuning methods, and relevant design optimization processes. The introduction of various optimization algorithms and their respective categories also takes place in this chapter. Chapter 3 delves into problem definition and modeling, outlining the problem addressed in the thesis and detailing the creation of a simplified nonlinear model using the Stiffness Evaluation Procedure (STEP) method. It also explores the use of the Particle Swarm Optimization (PSO) algorithm for tuning nonlinear stiffness. Moreover, it discusses strategies to handle constraints within the PSO algorithm. Moving on to Chapter 4, the results obtained from the analysis conducted in

this study are presented and discussed in depth, offering a comprehensive understanding of their significance and their connection to the research objectives and broader context. Finally, Chapter 5 serves as the conclusion, summarizing the findings, highlighting achievements, and suggesting potential areas for future research.

2

LITERATURE REVIEW

THIS chapter will investigate the concept of nonlinearity and its origins. The discussion will emphasize the dual nature of nonlinearity, demonstrating both its potential negative and positive effects. In addition, the significance of nonlinearity tuning will be examined, along with an overview of various tuning procedures. Following that, an in-depth analysis of design optimization and the accompanying optimization techniques will be performed. This analysis will divide optimization algorithms into two categories: gradient-based and stochastic optimization techniques. The latter will be further categorized, with each group receiving a thorough explanation.

2.1. GENERAL FEATURES OF MICRO- AND NANO-SCALE STRUCTURES

Micro- and nano-scale devices have emerged as invaluable tools with a wide array of applications across diverse industries. These devices, typically ranging from nanometers to micrometers in size, offer a host of advantages. In fields such as electronics [3, 4], healthcare [5, 6], and materials science [7, 8], they have revolutionized the way we interact with and manipulate the physical world. From high-precision sensors and actuators [9, 10] to compact signal processors [11, 12], these devices have proven their worth, often outperforming their macro-scale counterparts. Their compact size, existence of surface tension effects [8], having a molecular construction other than a bulk continuum structure and atomic effects [13], electrical properties, precision, and mobility [14] contribute significantly to their relevance in modern technology.

Micro- and nano-scale devices encompass a wide range of applications, including accelerometers for airbag sensors [15, 16], inkjet printer heads [17, 18], gyroscopes [19, 20], computer disk drive heads [21], projection display chips [22], blood pressure sensors [23], optical switches [24], microvalves [25], and numerous others produced in large commercial quantities.

To harness the full potential of micro- and nano-scale devices, a comprehensive understanding of their mechanical and dynamical behavior is paramount for designing devices in these scale. Without a grasp of these intricacies, it's challenging to exploit

their advantages fully. This understanding serves as the foundation for making these devices more reliable, efficient, and tailored to specific applications. Characterizing and controlling their dynamic behavior can also have significant applications in fields like medicine [26] , biology [27], and energy [28].

Modeling and optimization techniques play a pivotal role in realizing the potential of micro- and nano-scale devices. Through sophisticated simulations and mathematical models, engineers and scientists can predict device behavior, identify limitations, and fine-tune designs. By optimizing parameters such as material composition and geometry, these devices can be tailored to meet specific requirements and achieve unprecedented levels of performance. Modeling and optimization, therefore, are the keys to unlocking the full potential of micro- and nano-scale devices in our increasingly miniaturized world.

Two-dimensional (2D) materials and membranes have gained substantial attention in recent years for their unique and promising properties. These atomically-thin structures, often composed of a single layer of atoms, exhibit remarkable mechanical, electrical, and thermal characteristics that set them apart from their bulk counterparts [29]. Graphene, the poster child of 2D materials, possesses exceptional conductivity, strength, and flexibility [30].

Graphene finds applications in a variety of fields. In materials science, graphene serves as a reinforcement material in composites, enhancing their strength and durability [31]. Moreover, its high surface area and exceptional gas barrier properties enable its use in applications such as sensors [32], and energy storage systems [33], further illustrating its versatility and potential in numerous industries. In a recent study [34], the authors proposed a novel method for measuring the nanomotion of individual bacteria in their aqueous growing environment, using drums composed of ultrathin bilayer graphene. They showed that graphene drums can be used for antibiotic susceptibility testing with single-cell sensitivity, by monitoring changes in nanomotion in response to the administration of antibiotics in real time.

In the realm of micro- and nano-scale devices, the rapid emergence of nonlinearity stands as a remarkable and distinguishing feature. As these devices continue to shrink in size, their behavior deviates significantly from the linear, predictable patterns observed in macro-scale systems [35]. Nano and micro-scale devices more readily transition into the nonlinear regime due to factors like increased surface area-to-volume ratios, reduced dimensionality, and the dominance of surface forces. These factors collectively make nonlinear behavior more pronounced and lead to a rapid onset of nonlinear effects in small-scale systems. This phenomenon can be attributed to the intimate interplay between physical forces and material properties at the micro- and nano-scales.

2.2. LINEARITY VS. NONLINEARITY

2.2.1. LINEARITY

In the mathematical realm, linearity is a fundamental concept that extends its influence across various disciplines, including mechanical engineering. A system is deemed linear

when it adheres to the principles of superposition and homogeneity. In simpler terms, linearity implies that doubling the input produces a twofold increase in the output, and the system's response to a combination of inputs is the sum of its responses to each input individually. In fact, superposition means that if we have a linear system that responds to inputs x and y with outputs $f(x)$ and $f(y)$, then it will respond to the sum of inputs $x+y$ with the sum of outputs $f(x)+f(y)$. Additionally, homogeneity means that if we have a linear system that responds to input x with output $f(x)$, then it will respond to a scaled input αx with a scaled output $\alpha f(x)$, where α is a constant.

Translating this mathematical notion to the field of mechanical engineering, linearity manifests itself in the behavior of materials and structures. The foundation of many linear systems in mechanics is laid upon Hooke's Law, which posits a direct proportionality between the applied force and the resulting deformation. This adherence to proportionality simplifies the mathematical modeling of mechanical structures, as it allows engineers to employ linear algebraic equations to predict and analyze the system's response under different loading conditions.

Linear systems are characterized by a predictability and simplicity that greatly facilitates analysis. The application of linear models becomes especially valuable in the preliminary design and analysis phases, providing engineers with a straightforward framework to assess the performance of structures.

A mechanical system can be modeled as a mass and spring system (see Figure 2.1a), where a linear spring is used for simplicity. Hooke's law states that the force required to extend or compress a spring by a certain distance x is linearly related to that distance, given by $F = k_l x$. Here, k_l denotes the linear stiffness of the spring, and x is assumed to be relatively small. This translates that the force and displacement are directly proportional to each other. In the Figure 2.1b, we observe a plot depicting the relationship between force and displacement for a linear system. This plot shows that any changes in the input (displacement) are directly proportional to changes in the output (force). In other words, as we increase or decrease the displacement, the force responds in a predictable and linear manner, resulting in a straight-line graph. This characteristic of linearity is a fundamental property of the system, where the slope of the line represents its stiffness or compliance.

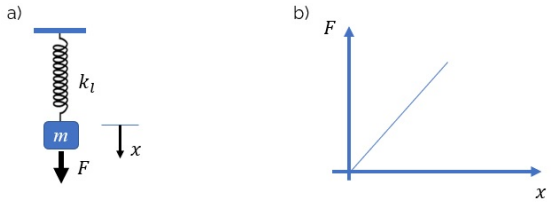

Figure 2.1.: Linearity in mechanical systems. a) Schematic of a mass-spring system featuring a linear spring. b) Force-displacement curve of a linear system shown in Figure 2.1a. Here, any changes in force are directly proportional to changes in displacement.

The equation of the motion for a linear mass-spring system can be written as

$$m\ddot{x} + k_l x = F \tag{2.1}$$

where m represents mass of the system and over-dot denotes differentiation with respect to time t.

However, it's crucial to acknowledge that linearity has its limitations, as real-world materials and structures can deviate from linear behavior and exhibit nonlinearity under specific conditions.

Yet, as we explore more demanding applications, acknowledging and addressing nonlinearities becomes imperative for a comprehensive and accurate understanding of mechanical behavior. This sets the stage for a discussion on nonlinear systems and their unique characteristics and challenges in the realm of mechanical engineering.

2.2.2. NONLINEARITY

A system is categorized as nonlinear when it departs from the principles of superposition and homogeneity. In more specific terms, nonlinearity arises when the system lacks proportionality between input and output. For example, doubling the input does not lead to a straightforward doubling of the output.

In a mechanical context, nonlinearity manifests as a departure from Hooke's Law. This means that changes in displacement are not directly proportional to changes in the inputs, underscoring the system's nonlinear behavior (see Figure 2.2b).

The nonlinearity inherent in many physical systems presents a significant challenge in their behavior. It results in various practical implications, including complex and unpredictable system responses such as chaotic behavior in dynamic systems [36, 37], the onset of resonance [38, 39], difficulties in control and stability analysis [40, 41], and a demand for specialized modeling and analysis techniques to precisely characterize and forecast system behavior [42].

In order to enhance the precision of modeling a nonlinear system, one can introduce a nonlinear spring k_{nl}, as illustrated in Figure 2.2a. Unlike a linear relationship, which results in a straight line on a graph, a nonlinear relationship produces a curve, as depicted in Figure 2.2b. The dotted line is associated with a linear system, while the non-dotted line represents a nonlinear system. The deviation from the linear curve is a consequence of introducing nonlinear stiffness (k_{nl}), which amplifies the overall system stiffness, leading to an augmented slope in the tangent line on the curve.

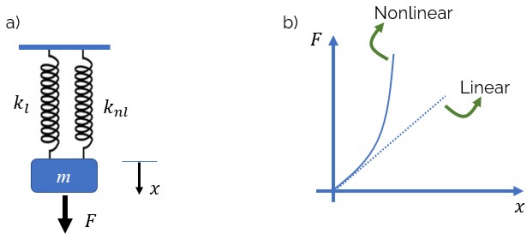

Figure 2.2.: Nonlinearity in the context of mechanical systems. a) Schematic of a mass-spring system that comprises both linear and nonlinear springs. b) Force-displacement curve of a nonlinear system as shown in Figure 2.2a. The deviation from the linear curve results from the introduction of nonlinear stiffness k_{nl}, which enhances the overall system stiffness, manifesting as an increased slope of the tangent line on the curve.

In most applications, a nonlinear mechanical system can often be simplified by the following equation:

$$m\ddot{x} + k_l x + k_{nl} x^3 = F \tag{2.2}$$

It signifies that the resistance to deformation in the system is nonlinear and proportional to the cube of the displacement x. In other words, as the system is displaced from its equilibrium position, the force required to deform it further is not directly proportional to the displacement but rather increases cubically. This cubic term accounts for the nonlinear behavior of the system and can capture phenomena where the stiffness of the system varies significantly with the magnitude of deformation.

It's important to note that nonlinearity in mechanical systems cannot always be solely represented by the term x^3 as shown in Equation (2.2). In practice, nonlinearity can take various forms, such as cubic, quadratic, or other functional relationships [43, 44]. To accurately capture the system's behavior, these variations may necessitate alternative modeling approaches. This flexibility in modeling is essential for addressing a wide range of nonlinear phenomena that may arise in different applications.

Micro- and nano-scale devices exhibit linear behavior at low vibrational amplitudes. However, as the amplitude increases, nonlinear effects become prominent, causing these devices to enter a nonlinear regime where a linear approximation is no longer suitable. Nonlinearity is a common feature of tiny structures and has significant implications for device performance and design, especially in the context of micro- and nano-scale devices.

Recognizing and understanding nonlinearity in micro- and nano-scale systems is pivotal for accurate modeling and analysis, as it necessitates distinct approaches and tools to describe and predict their behavior. As a result, a clear understanding of nonlinearity is essential for effectively using micro- and nano-scale structures.

2.3. NONLINEARITY SOURCES

Nonlinearity can be attributed to various system characteristics, including geometry, material, boundary, and loading.

A brief description of nonlinear sources is provided as follows.

- **Geometrical Nonlinearity:** This type of nonlinearity occurs when a structure undergoes significant deformations under external load. For example, a thin-walled structure that experiences substantial bending may exhibit nonlinear behavior due to these geometric changes [45].

- **Material Nonlinearity:** Materials frequently exhibit nonlinear behavior, which is a crucial aspect of material science and engineering. This nonlinearity arises when a material's response to external forces deviates from a linear, predictable pattern [46]. For instance, metals can endure plastic deformation beyond their elastic limit, meaning that when subjected to substantial stress, they change shape permanently. This plasticity introduces material nonlinearity, causing shifts in stiffness and behavior [47]. Beyond plasticity, other factors can contribute to material nonlinearity, such as strain hardening, where a material becomes harder as it deforms [48], or viscoelasticity, where materials display both viscous and elastic properties, resulting in time-dependent responses [49].

- **Boundary Conditions:** Kinematic or geometric constraints at the structure's boundaries can induce nonlinear behavior [50]. For example, a flexible cable under tension may exhibit nonlinear behavior as it approaches a critical tension point. This nonlinearity can be attributed to constraints imposed at its endpoints, including the possibility of cable slippage. Likewise, a beam can undergo nonlinear deformation when subjected to special imperfect boundary conditions [51].

- **Loading Conditions:** Different loading conditions, ranging from mechanical forces to thermal gradients, can lead to intricate and nonlinear responses in structures and materials. For instance impact loading, can lead to nonlinear behavior in a structure [52]. When a structure is subjected to impact loading, it experiences rapid, high-energy forces or impulses that deviate significantly from gradual, steady-state loading [53]. This sudden and intense force application can induce nonlinear responses in the structure, often resulting in dynamic deformations and stress distributions that differ from what would be expected under more gradual loading.

When these sources of nonlinearity are present in a structure, the system's behavior deviates from linearity. In summary, both geometric nonlinearity and nonlinear material behavior are vital considerations in mechanical engineering and the dynamics of micro- and nano-scale structures.

Understanding and accurately modeling these sources of nonlinearity is essential for the design and analysis of many mechanical systems. In the following sections, we will delve into further detail on geometric and material nonlinearities.

2.3.1. GEOMETRIC NONLINEARITY

Geometric nonlinearity arises whenever the magnitude of displacements significantly influences the response of a structure. This phenomenon occurs when deformations, either in the form of large deflections or rotations, reach a point where they can no longer be neglected. In such cases, the traditional linear assumptions about the relationship between loads and deformations are no longer valid, and the structural response becomes inherently nonlinear. Geometric nonlinearity is a critical consideration in the analysis and design of various structures, particularly in scenarios where deformations cannot be approximated as small.

When the stiffness of the part significantly changes during the deformation process due to alterations in geometry, one must consider geometric nonlinearity from the perspective of stiffness. In such cases, the response of the structure deviates from traditional linear assumptions, leading to geometric nonlinearity. This geometric nonlinearity can manifest in two distinct ways: softening or hardening behavior.

In cases of softening behavior, as a structure deforms, it becomes less resistant to additional deformation (see Figure 2.3). This is often observed in structures that loosen or exhibit a reduction in stiffness as they deform. Softening behavior can lead to instability and even structural failure if not appropriately addressed.

On the other hand, hardening behavior occurs when a structure becomes stiffer as it deforms (see Figure 2.3). This phenomenon is typically associated with structures that possess elements or features that stiffen or become more resistant to deformation as they experience greater loads or displacements. Hardening behavior can be advantageous in certain applications, such as in energy-absorbing structures designed to withstand impact forces [54].

Understanding whether geometric nonlinearity results in softening or hardening behavior is crucial for accurate structural analysis and design. It plays a vital role in assessing the stability and safety of structures, especially when they experience significant deformations.

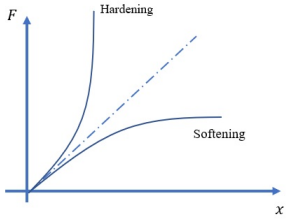

Figure 2.3.: Force-displacement curve in a mechanical system with geometric nonlinearity. Here, when the nonlinear stiffness in Equation (2.2) is positive, a hardening curve manifests, while negative nonlinear stiffness leads to softening effects. The dashed line corresponds to the force-displacement curve for a linear system.

2.3.2. MATERIAL NONLINEARITY

Material nonlinearity is a crucial aspect in understanding the behavior of structures and systems, particularly in the field of mechanics and materials science. Material nonlinearity can be directly related to the molecular structure of a material [55]. The molecular structure and arrangement of atoms within a material significantly influence its mechanical behavior. Material nonlinearity refers to the situation where the response of a material does not follow a linear relationship between stress (applied force) and strain (resulting deformation). Instead, material nonlinearity signifies that the stress-strain relationship deviates from Hooke's Law, which describes the linear behavior of elastic materials.

Nonlinear material behavior can be described using stress-strain curves, illustrating the relationship between stress and strain for a specific material (see Figure 2.4). These curves are used to determine essential mechanical properties of the material, including yield stress (σ_y) and ultimate stress (σ_u). In Figure 2.4, the material exhibits linear behavior up to the yield stress point, commonly referred to as the elastic deformation region. During this phase, the material behaves predictably and responds proportionally to applied loads. However, beyond the yield stress point, the material undergoes a transition into a nonlinear regime. In this nonlinear range, the material's response becomes increasingly complex, and its behavior no longer adheres to the linear principles observed during elastic deformation. Here, the material might exhibit various nonlinear effects, such as plastic deformation, strain hardening, or other forms of nonlinearity, which are associated with changes in its microstructure and properties.

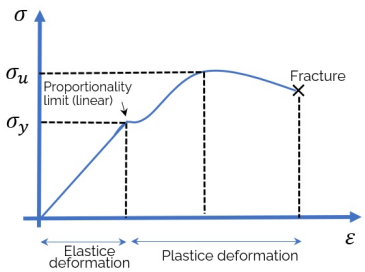

Figure 2.4.: The stress-strain curve of a mechanical system with material nonlinearity. The material exhibits linear behavior in the elastic deformation region up to the yield stress point. Beyond this point, a transition occurs, leading to nonlinear behavior in the material's response, and a departure from the linear principles observed during elastic deformation.

In summary, material nonlinearity is a fundamental aspect of structural mechanics. Its presence in materials can significantly impact how structures respond to forces and deformations, making it a critical consideration in various engineering and design applications. Engineers and researchers employ specialized testing, analysis, and modeling techniques to account for material nonlinearity and ensure the safety and reliability of structures and components in practical scenarios.

2.4. DIFFERNET ASPECTS OF NONLINEARITY

Nonlinear systems can exhibit complex and intriguing behaviors, including chaos and bifurcation. Chaos, exemplified by its unpredictable dynamics, can introduce challenges and opportunities in various applications, as shown in recent studies [56]. Bifurcation represents a fundamental shift in a system's behavior as a control parameter varies, resulting in the emergence of new stable or oscillatory states, as demonstrated in related research [57]. Therefore, the analysis of nonlinear systems is pivotal for advancing knowledge and applications in these domains.

Initially, engineering research on nonlinearities primarily focused on nullifying or mitigating their effects [58]. However, recent research in this field explores the use of nonlinearity to enhance performance [59] .

The central inquiry revolves around the dual nature of nonlinearity, encompassing both advantageous and detrimental attributes. Nonlinearity may be deliberately selected for its beneficial qualities or strategically employed to alleviate its drawbacks.

Nonlinearity introduces a spectrum of challenges and limitations. In this context, attention will be directed towards elucidating two noteworthy aspects of its influence.

- **Uncertainty:** Nonlinearity in a system leads to uncertainty, as changes in the inputs don't result in proportional changes in the outputs. Consequently, the system's behavior becomes unpredictable [60, 61].

- **A-F Effect:** Many micro- and nano-scale structures must operate at specific resonant frequencies, crucial for functions like timing devices [62], filter frequencies [63], and resonant accelerometers [64]. These frequencies depend on the device's amplitude. In reference [65], the authors explored the nonlinear free vibration of a prestressed orthotropic membrane at large amplitudes. They derived an approximate analytical expression indicating that frequency is proportional to the square of the amplitude. Therefore, even slight changes in amplitude can result in significant frequency fluctuations.

On the contrary, nonlinearity is accompanied by numerous benefits. Within this framework, two primary facets of its influence will be explained.

- **Amplitude Stabilization:** Nonlinear coupling of resonant modes within a single structure can stabilize the amplitude and, consequently, the frequency at a desired mode. In a study by Defoort et al. [66], researchers examined a nanomechanical self-sustained oscillator synchronized with an external harmonic drive. Their results provide insights into unexplored aspects of synchronization phenomena and propose a novel method for enhancing amplitude stability in oscillators.

- **Determining Mechanical Properties:** Davidovikj et al. [35] demonstrated the use of the nonlinear response of a suspended 2D material membrane to determine Youngs modulus. This method is rapid, non-invasive, and provides a foundation for evaluating the mechanical properties of 2D materials at high frequencies.

In a nutshell, the capacity to adjust and optimize nonlinearity effects can improve system performance while also alleviating the constraints of designing structures at the micro- and nano-scale.

2.5. TUNING NONLINEARITY

Tuning Nonlinearity refers to the deliberate adjustment or manipulation of nonlinear behavior within a system. This process involves modifying various parameters or characteristics to achieve specific desired nonlinear effects or responses [67]. Nonlinearity tuning can be used to optimize system performance [68], control chaotic behavior [69], enhance energy transfer [70], or achieve other tailored outcomes, depending on the application and objectives. Nonlinearity can be tuned or controlled using various methods based on the system's specific characteristics. Here are two general techniques:

- **Using External Forces (Fields):** Altering certain material or system properties by applying external fields. For example, applying an electric field can modify a material's electrical conductivity, and a magnetic field can change its magnetic properties.

- **Design Optimization (Mechanical Design):** Design optimization is a systematic process employed in various fields, including engineering, to identify the optimal design or solution that aligns with specific criteria and objectives while taking into account various constraints. This process leverages mathematical and computational techniques to explore and assess various design alternatives, enabling the adjustment of design parameters and informed decision-making to optimize a product or system's performance, efficiency, and other desired attributes. The benefits of design optimization extend to improved designs, cost savings, reduced resource utilization, and enhanced product functionality, ultimately leading to more efficient and effective solutions across diverse applications [71, 72].

In the following sub-sections, the complexities of tuning a system using external forces and design optimization (mechanical design) will be delved into.

2.5.1. TUNING THROUGH EXTERNAL FORCES (FIELDS)

There are various techniques for applying external fields to a system, depending on the system's nature and the type of field involved. For instance, electric fields [73] can be generated by applying voltage across a material, while magnetic fields can be produced using magnets or coils of wire. In reference [67], the authors explored an electrostatic method for expanding the dynamic range of nanomechanical resonators used as sensors by modifying their nonlinearity.

The advantages of tuning with external fields include the ability to control a system's properties without physically altering it and achieving precise and reversible changes in the system's behavior. However, this approach may be constrained by the strength and range of the external field and the system's sensitivity to external perturbations.

2.5.2. TUNING VIA MECHANICAL DESIGN

Mechanical design is making adjustments to system components, such as springs and mechanical parts, to optimize their behavior and achieve desired performance. The goal is to maximize performance while minimizing energy losses, vibrations, and other negative effects.

In mechanical design, tuning involves a comprehensive analysis of the system's behavior, the identification of factors influencing its performance, and the implementation of appropriate adjustments to mechanical components. These techniques may include alterations to component size, shape, or other parameters to enhance overall system performance [74].

The advantages of tuning through mechanical design include optimizing system performanceand achieving precise control over the system's behavior. However, this approach may require specialized knowledge and equipment [74]. Overall, mechanical design for tuning proves to be a valuable tool for enhancing the performance of mechanical systems and finds widespread applications across various fields.

Every system has a set of inputs, which are the variables or unknowns of the problem. Changing or tuning these inputs allows us to maximize or minimize the system's output. Another critical aspect is the set of constraints, which limit the system. Constraints can be considered as secondary inputs, but their impact differs from primary inputs. They define the system's limits and help identify feasible solutions. Constraints determine which input setups are valid and which are not. The objective can be calculated for any input set.

After identifying the inputs, outputs, and constraints, the next step is to formulate the system as an optimization problem. To achieve this, we employ optimization algorithms, which are mathematical models or computer programs designed to find the optimal values for the problem's variables. These algorithms aim to maximize or minimize the output while adhering to the defined constraints. In essence, optimization algorithms explore the vast solution space, searching through all possible combinations of inputs.

Designing with optimization algorithms offers the advantages of rapid modeling, automated simulation, and error reduction in the design process. However, the primary challenge lies in the requirement of a complex optimization algorithm capable of efficiently identifying the optimal design.

Two common categories of optimization algorithms are:

- **Conventional Optimization Algorithms (Gradient-Based)**
- **Modern (Stochastic) Optimization Algorithms**

In the following sections, each of these optimization algorithms will be explored in detail. Additionally, the advantages and disadvantages of each approach will be discussed.

2.5.2.1. CONVENTIONAL OPTIMIZATION ALGORITHMS (GRADIENT-BASED)

One of the most widely recognized conventional optimization algorithms is known as gradient descent. The gradient, in this context, is a function that points in the direction of the steepest increase in the landscape [75, 76]. It iteratively moves from one point to the next, considering the negative value of the gradient. In simpler terms, it gradually converges towards the minimum of the search landscape, especially in unimodal landscapes, where any starting point eventually leads to the global minimum when using the gradient algorithm (see Figure 2.5).

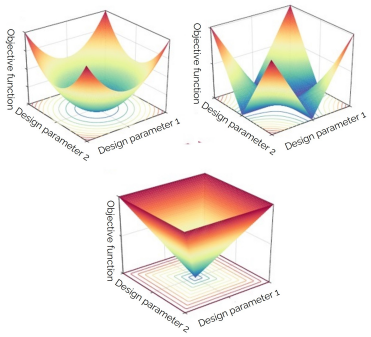

Figure 2.5.: Three unimodal landscapes. It is evident that all the points in these three plots converge to the global minimum.

In a multimodal landscape (see Figure 2.6) characterized by multiple local solutions, the gradient descent algorithm often leads to a local minimum. Unfortunately, this implies that the algorithm assumes a local solution is the best global solution, a phenomenon known as "local optima stagnation" or "local optimal entrapment" in the field of optimization.

The efficiency of the gradient descent algorithm is highly dependent on the initial starting point. To address this issue, one approach to improve its efficiency is to run the algorithm multiple times with random initial solutions.

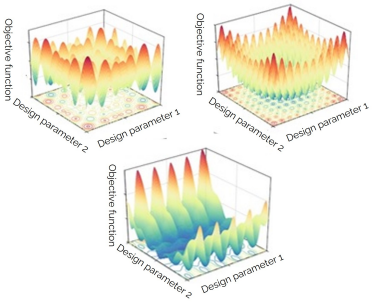

Figure 2.6.: Three multimodal landscapes, where all the points in these plots exhibit multiple local minima, posing a challenge in locating the global optimum.

Imagine the time-consuming process of running the gradient descent algorithm multiple times with different initial positions, which can be especially burdensome when tackling complex problems with numerous design variables and constraints, resulting in a significantly larger design space (see Figure 2.7).

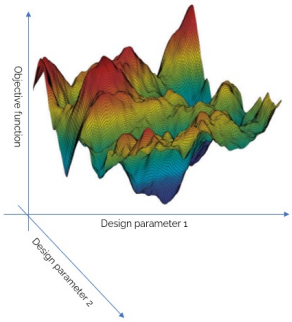

Figure 2.7.: Example of design space for a problem with two design variables. Even with just two design variables, we can encounter a challenging design space, which makes finding the global optimum a formidable task.

Extensive research has been conducted in the field of structural optimization utilizing gradient-based optimization methods [77, 78]. Shaw et al. [79] introduced an innovative gradient-based optimization method for tailoring the nonlinear behaviors of a clamped-clamped beam. They demonstrated a computational approach enabling systematic manipulation and optimization of nonlinear responses in mechanical structures. Structural optimization was applied to modify the parameter that most accurately represents the core nonlinearity of the reduced-order model.

It should be noted that the solutions obtained in their study depend on the initial design, and there is no guarantee that they represent global optima. However, multiple optimization iterations demonstrate that the approach is relatively stable, and any potential performance gains from redesigning the structure are expected to be minimal at best.

In a nutshell, gradient-based optimization techniques offer reliability in consistently finding the same solution in each run and fast convergence. However, these methods suffer from issues such as local optima stagnation, low probability of finding the global optimum in real-world problems, dependence on the initial solution, and the need to calculate the gradient, which might be unknown or ill-defined when solving real-world problems. Because of these limitations, I have introduced another method, which is a modern (stochastic) optimization algorithm.

2.5.2.2. MODERN (STOCHASTIC) OPTIMIZATION ALGORITHMS

Stochastic optimization algorithms are a class of techniques designed to address complex real-world problems characterized by uncertainty and randomness. The modern

optimization algorithms are equipped with random components and find different solutions in each run, even when the starting point is similar [80]. Stochastic optimization algorithms are normally run multiple times, and in each run, they search for the global optimum until the satisfaction of an end condition. This condition might be a pre-defined maximum number of steps or when the algorithm finds a reasonable objective value that we expect.

In reference [81], the authors introduced a specialized stochastic method designed for the mechanical dimensioning of overhead power distribution lines. This innovative approach serves the specific purpose of determining the mechanical dimensions of such power lines, showcasing a tailored solution for this particular task.

The advantages of stochastic algorithms are high local optima avoidance, high probability of finding the global optimum, low dependency on the initial solution , and the gradient-free mechanism. However, the search speed are lower than deterministic algorithms and they find different answers in the run. Undoubtedly, the benefits of employing stochastic algorithms far surpass any drawbacks they may have. I intend to categorize stochastic optimization algorithms in the upcoming discussion.

CATEGORIES OF STOCHASTIC OPTIMIZATION ALGORITHMS

In the most well-regarded classification, stochastic optimization algorithms are divided into two classes. If one particle searches for the global optimum, the entire search process is individual-based. If more than one particle look for the global optimum, however, the search process is population-based [82].

The advantage of individual base algorithm is the need for the minimum number of function evaluations. The number of function evaluations is equal to the number of iterations. However, such techniques suffer from local optimal stagnation or premature convergence. This is because a single solution is very likely to be trapped in local solutions because there is a lot of local solutions when solving real-world problems.

By contrast, population-based techniques benefit from high exploration of the search space and low probability of local optimal entrapment. If a candidate solution goes inside the local optimum, other solution will assist to avoid it in the next iteration. As drawbacks, such algorithms require more function evaluations and are computationally more expensive [83].

There is no doubt that the advantages of population-based algorithms outweigh the drawbacks. High local optima avoidance and exploration make population-based algorithms a better solution to real-world problems as compared to the individual-based algorithms.

Population-based algorithms can be categorized into three classes: evolution-based, physics-based, and swarm-based methods. In the upcoming section, brief descriptions of each of these classes will be provided. Subsequently, a comparison will be made to determine which one is better suited for addressing the specific problem presented in this thesis.

Evolution-based methods are inspired by the laws of natural evolution. The search process starts with a randomly generated population which is evolved over subsequent generations. The strength of these methods is that the best individuals are always combined together to form the next generations of individuals. This allows the population to be optimized over the course of generations. The most popular evolution-inspired technique is Genetic Algorithms (GA) that simulates the Darwinian theory of Evolution [84, 85].

Physics-based algorithms refer to methods that incorporate principles from physics or other natural phenomena into the optimization process or simulation. These algorithms often leverage physical laws and principles to guide the search for optimal solutions or to model complex systems accurately [86, 87].

Swarm-based techniques mimic the social behaviors of groups of animals. Popular and most well-regarded techniques in this class are: Particle Swarm Optimization (PSO) and Ant Colony Optimisation (ACO) [88, 89]. Particle Swarm Optimization algorithm has been widely applied to various optimization problems. It's a popular and efficient algorithm that can often find good solutions in complex, high-dimensional search spaces.

Highlighting the advantages of Particle Swarm Optimization (PSO) algorithms over Evolutionary-Based Algorithms, PSO is notably recognized for its ease of implementation and efficiency. Compared to many Evolutionary-Based algorithms like Genetic Algorithms (GAs), PSO is relatively easier to implement and has fewer parameters to tune. This simplicity can save time in setting up and running experiments. Furthermore, PSO is often more computationally efficient, as it requires fewer function evaluations than GAs, making it a faster optimization method.

Emphasizing the benefits of Particle Swarm Optimization (PSO) algorithms over Physics-Based methods, a notable advantage of PSO lies in its independence from explicit physical models. Unlike Physics-Based methods, which rely on a comprehensive understanding of the physical processes and governing equations, PSO is applicable to a broader range of problems where the underlying physics may not be well understood or involves intricate interactions. Additionally, PSO exhibits less sensitivity to parameterization compared to Physics-Based methods, where fine-tuning parameters can be a more challenging and time-consuming task. This characteristic further underscores the versatility and efficiency of PSO in addressing problems with varying degrees of complexity.

Therefore, PSO's efficiency, global optimization capabilities, and ease of implementation make it a well-suited choice for addressing the specific challenges and objectives of my thesis.

EXPLORATION VS. EXPLOITATION

To solve optimization problems, algorithms employ two conflicting and fundamental phases: exploration and exploitation. These two phases are essential to find an accurate estimation of the global optimum for any given optimization problem [90, 91].

In the exploration phase, an algorithm abruptly changes the candidate solutions to ensure that they explore different regions of the search landscape.

In the exploitation phase, the magnitude of changes in the solutions is much lower than that in the exploration phase. In other words, the search is done locally around the most promising solutions found in the exploration phase.

What makes the process of designing and utilizing population-based algorithms difficult is that the exploration and exploitation phases are in conflict. A mere exploratory behavior mostly results in finding very poor solutions. By contrast, more exploitative behavior results in trapping local solution because the algorithm never get the chance to change the solution abruptly.

3

METHODS AND PROBLEM DEFINITION

THIS chapter provides an in-depth exploration of methodologies employed in the optimization of micro- and nano-scale devices. To facilitate this, the Reduced Order Model (ROM) is initially introduced as a crucial tool for simplifying systems with infinite Degrees of Freedom (DOF) to a single DOF, enhancing manageability and analytical capabilities. Subsequently, the STEP method, a specialized ROM, is presented for constructing nonlinear ROM models and determining the nonlinear stiffness. The optimization of a simplified single DOF system necessitates the application of an optimization algorithm capable of handling the procedure. In this context, the Particle Swarm Optimization (PSO) is employed, as conventional gradient-based methods prove inadequate when dealing with a large number of design parameters. Furthermore, Discrete Particle Swarm Optimization (DPSO) and Binary Particle Swarm Optimization (BPSO) are introduced for problems involving discrete and binary design parameters, respectively. Moreover, considering that various problems may encounter different limitations and constraints, the penalty function is introduced as an effective method for addressing constraints within the scope of this thesis.

To integrate these methods into a unified framework addressing a defined design problem, the optimization of the nonlinear stiffness of a circular membrane is pursued by introducing circular voids. This process involves using the STEP method to transform a complex geometry into a Single Degree of Freedom (SDOF) mass-spring system. Subsequently, the Particle Swarm Optimization (PSO) algorithm is employed to iteratively adjust the geometry parameters, implementing optimization logic to identify the optimal design that either minimizes or maximizes the nonlinear stiffness of the device.

3.1. REDUCED ORDER MODELLING

In real-world scenarios, challenges arise with the presence of infinite degrees of freedom (DOF) in problems, complicating the prediction of structural behavior. To address this challenge, the reduction of DOF is achieved through various approaches. The process of

simplifying a complex system by decreasing its degrees of freedom to a smaller number is also denoted as Reduced Order Modelling (ROM).

Consider a circular membrane with an infinite DOFs (see Figure 3.1a). The investigation of this system's behavior and the resolution of the corresponding equations of motion pose challenges due to the infinite DOFs. To address this, the equations of motion for the membrane can undergo discretization using methods like the finite element method (FEM). This discretization process reduces the infinite dimensionality of the equations to a finite yet substantial number of DOFs (see Figure 3.1b). However, when dealing with an optimization problem requiring numerous system evaluations, even this finite DOFs model may involve solving for less crucial, time-consuming details. Hence, further simplification becomes necessary. Consequently, utilizing a mass-spring system as a model for the system, capable of effectively capturing the fundamental mechanical features, presents significant advantages (see Figure 3.1c).

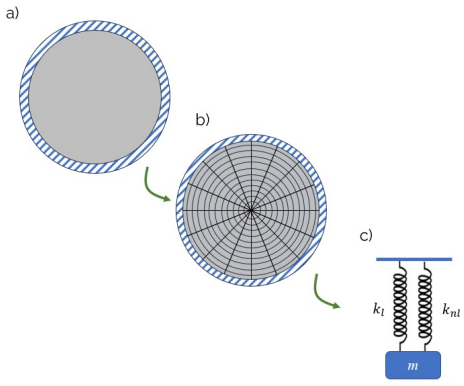

Figure 3.1.: Schematic of a reduced order model for a circular membrane: a) A circular membrane with an infinite number of degrees of freedom. b) A meshed model of the membrane (as shown in Figure 3.1a) with a finite number of degrees of freedom. c) A simplified model (based on Figure 3.1b) representing the membrane as a mass and spring system, comprising both linear and nonlinear springs.

The vibration behavior exhibited by continuum structures, arising from the inherent infinite Degrees of Freedom (DOF) in the system, entails intricate mechanical phenomena necessitating analytical solutions for optimal accuracy. However, the applicability of these analytical solutions is contingent upon various factors, including geometry, type of loading, and other specific characteristics inherent to the problem at hand. Practical implementations often reveal that only a limited subset of the infinite vibrational modes of a structure proves influential in predicting its dynamic behavior, as demonstrated in references [92, 93].

Eigenmodes represent characteristic vibration patterns at specific frequencies. In modal analysis, the careful selection of eigenmodes is significant, as each mode corresponds to distinct vibrational frequencies. Leveraging these eigenmodes enables the creation of

a linear reduced-order model, facilitating computational efficiency in solving complex structural dynamics problems. This methodology is notably efficacious in the realm of linear systems. However, its application becomes more intricate when confronted with nonlinear systems, necessitating a nuanced consideration of nonlinear behavior. Consequently, modal analysis emerges as a valuable tool for systematically reducing the number of Degrees of Freedom (DOFs) and extracting essential insights into the structural dynamics.

In the formulation of a nonlinear reduced-order model, the incorporation of nonlinear terms into the simplified equations becomes imperative. Quadratic and cubic terms are frequently favored owing to their adept approximations achievable through the Taylor series, as noted by Shaw [93]. The derivation of nonlinear terms in the reduced equations involves extracting them from the comprehensive set of equations representing the entire system. Subsequently, the computation of nonlinearities for each eigenmode becomes a crucial step in developing an accurate representation of the nonlinear structural response.

Various techniques exist for reducing the Degrees of Freedom (DOFs) of a system and identifying nonlinear stiffness in the modal domain. These techniques encompass analytical approaches and Finite Element Method (FEM)-based approaches.

3.1.1. ANALYTIC APPROACHES

Structures that can be represented using continuous mathematical functions can be analyzed through analytical methods. In theoretical terms, the displacement field of a structure can be approximated by incorporating contributions from all of its infinite mode shapes. Nevertheless, it has been demonstrated that for the majority of dynamical problems, only a limited number of mode shapes are necessary to faithfully reproduce the displacement field behavior [94–97]. Utilizing a reduced number of modes significantly diminishes the Degrees of Freedom (DOFs) of the system. These methods offer the advantage of providing a mathematical governing equation for the dynamics of the system, which, in specific cases, can be solved analytically, yielding an analytical relationship for the problem.

In instances where an analytical solution is not feasible, the analytical governing equation still provides insights into certain behavioral aspects of the structure with minimal effort. Nevertheless, when dealing with a complex structure, the extraction of mode shapes becomes a challenging task and, in many instances, analytically unattainable. Consequently, this method is severely restricted to simple geometries and limited applications.

3.1.2. FEM-BASED APPROACHES

On the contrary, for complex structures, the recommended approach is to use a finite element method (FEM)-based method. Finite Element Method (FEM)-based approaches are numerical techniques widely employed for analyzing and simulating the behavior of structures. The fundamental logic behind FEM involves subdividing a complex structure into smaller, simpler elements that are interconnected at nodes. By applying governing

equations to each element, the overall behavior of the entire structure can be systematically approximated. FEM allows for the examination of intricate structural details, making it a versatile tool in engineering analysis.

Several FEM-based methods exist, each with its specific applications and advantages. Notable methods include the Direct Stiffness Method (DSM), Substructure Method, and the Stiffness Evaluation Procedure (STEP) method. The DSM directly assembles the stiffness matrix of the entire structure [98, 99], while the substructure method breaks down a complex structure into substructures, solving them individually before assembling the results [100, 101].

In the context of this research, the STEP method is selected as a versatile and potent analytical tool, tailored for the examination of structural dynamics. This method serves as a robust platform for the investigation of nonlinear stiffness in structures, offering comprehensive insights into the intricate mechanical behavior of the system under consideration. The subsequent subsection delves into the specifics of the STEP method and its application in this parametric study.

3.1.2.1. STIFFNESS EVALUATION PROCEDURE (STEP)

The STEP method involves a systematic series of steps aimed at simplifying the dynamic analysis of a complex structure into a single-degree-of-freedom (SDOF) mass-spring system. A comprehensive overview of the sequential steps of this method is provided in Figure 3.2. Initially, a linear ROM is constructed based on the full nonlinear model, neglecting the system's nonlinearities. After defining the linear ROM, STEP utilizes information from the full nonlinear model to establish the nonlinear Reduced Order Model.

In essence, when the structure is linearized, the nonlinearities are not considered; instead, STEP employs information from both the linear and full nonlinear models (as indicated by the red lines in Figure 3.2) to construct a nonlinear reduced order model. Following the construction of the nonlinear reduced order model, the system's nonlinear stiffness can be determined.

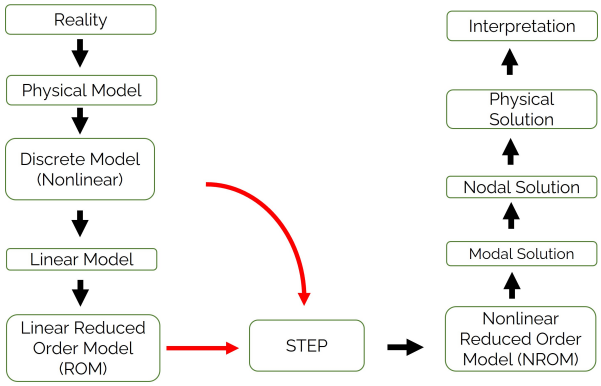

Figure 3.2.: The framework of the STEP approach for modeling nonlinear dynamics involves the utilization of both a linear reduced-order model and the nonlinearities extracted from the full nonlinear model to construct a comprehensive nonlinear reduced-order model [102].

The subsequent section offers an in-depth exploration of the STEP method, as detailed in reference [103]. It provides comprehensive insights into the framework, implementation in problem-solving scenarios, and mathematical underpinnings of the method.

In many problems, the fundamental mode governs the motion, allowing for the assumption that the structure can be approximated by its fundamental mode. Mathematically, it can be demonstrated that relying solely on the fundamental mode results in a Single Degree of Freedom (SDOF) mass-spring system (see Figure 3.3a). However, in reality, each mode has a nonlinear stiffness associated with it (see Figure 3.3b). When the structure is linearized for modal analysis, this critical information is lost. To obtain the nonlinear stiffness (as shown in (see Figure 3.3c)), we can solve the system statically by imposing a constant velocity, zero acceleration and prescribing a displacement Δx. Then, we assess the required force F_e. This solution can be used to calculate the nonlinear stiffness coefficient k_{nl}.

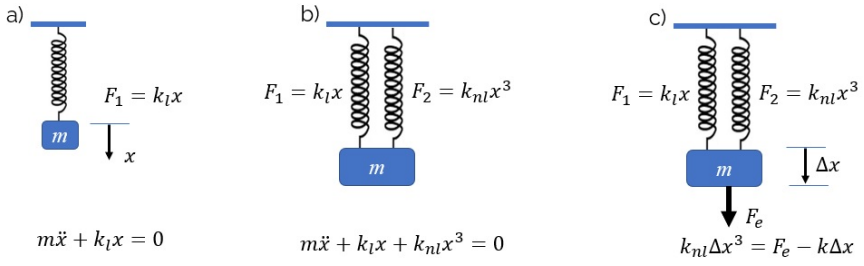

Figure 3.3.: STEP method: a) Linear uncoupled system obtained from modal analysis. b) In reality, nonlinear stiffness is present. c) The nonlinear stiffness can be identified by prescribing a modal displacement and evaluating the modal force.

Building upon the conceptual foundation laid out in the preceding discussion of the STEP method and its operational flowchart, the mathematical formulation is now explored. The equation of motion for a system characterized by multiple degrees of freedom, featuring both geometric nonlinearity and viscous damping, can be expressed as follows:

$$M\ddot{X}(t) + C\dot{X}(t) + KX(t) + \Gamma(X(t)) = F(t) \tag{3.1}$$

In the given equations, the displacement response vector is represented by X, the force excitation vector by F, the mass matrix by M, the proportional damping matrix by C, and the linear stiffness matrix by K.

The nonlinear stiffness force vector Γ comprises second and third order terms in X, which means it includes components that are proportional to the squares and cubes of the displacement vector X. These nonlinear terms become significant when the displacements are not small, and they are often encountered in systems exhibiting geometric nonlinearity. However, for small displacements, such as those in linear analysis, these nonlinear terms become negligible and can be approximated to be zero.

To streamline the analysis, an initial step entails the application of a modal coordinate transformation. This transformation aids in reducing the system's complexity by generating a set of modal equations. These interconnected modal equations exhibit fewer degrees of freedom compared to the original system. This methodology enhances the manageability and efficiency of the analysis for subsequent investigations. The modal coordinate transformation is executed as follows:

$$X = \Phi q \tag{3.2}$$

Here, Φ represents the eigenvectors obtained from Equation (3.1) without C, and q denotes the vector of modal coordinates. The following equations are derived by substituting Equation (3.2) into Equation (3.1).

$$\widetilde{M}\ddot{q} + \widetilde{C}\dot{q} + \widetilde{K}q + k_{nl}(q_1,\ q_2\,,\ ...,\ q_L) = \widetilde{F} \tag{3.3}$$

$$\widetilde{M} = \Phi^T M \Phi = [I] \tag{3.4}$$

$$\widetilde{C} = \Phi^T C \Phi = [2\zeta_r \omega_r] \tag{3.5}$$

$$\widetilde{K} = \Phi^T K \Phi = \left[\omega_r^2\right] \tag{3.6}$$

$$k_{nl} = \Phi^T \Gamma \tag{3.7}$$

$$\widetilde{F} = \Phi^T F \tag{3.8}$$

In the presented equations, the symbol ~ designates a transformed version of a matrix. The matrix $[I]$ represents the identity matrix, while Φ^T denotes the transpose of the matrix Φ.

In general, the solution includes a subset of L eigenvectors. Here, $q_1, q_2, \ldots, q_L$ are the components of the vector q, and ω_r denotes the undamped natural frequency. Additionally, ζ_r represents the damping ratio associated with a mode.

By expressing the nonlinear force vector in the following form

$$k_{nl}(q_1, q_2, ..., q_L) = \sum_{j=1}^{L}\sum_{k=j}^{L} a_{jk}^r q_j q_k + \sum_{j=1}^{L}\sum_{k=j}^{L}\sum_{l=k}^{L} b_{jkl}^r q_j q_k q_l, \quad r = 1, 2, ..., L \tag{3.9}$$

the challenge of determining nonlinear stiffness, which initially involved solving a vast set of simultaneous nonlinear equations, has been transformed into a problem characterized by straightforward algebraic relationships. To evaluate it, one must employ a novel method for solving for the coefficients a_{jk} and b_{jkl}.

The method for both linear and nonlinear static solutions relies on specifying nodal displacements to recover the applied forces at each node. In physical coordinates, the total forces at all nodes, denoted by F_T, can be represented as follows:

$$F_T = F_L + F_{NL} = KX_C + \Gamma(X_C) \tag{3.10}$$

where X_C is a prescribed physical displacement vector at the node, and F_L and F_{NL} are the linear and nonlinear components of the total force at the node, respectively. After obtaining the linear static solution, F_L is achieved by prescribing X_C. Thus, by making a prescription for X_C in the nonlinear static solution, F_T may be produced. After all, the nonlinear contribution F_{NL} is determined by deducting F_L from F_T, or

$$F_{NL} = \Gamma(X_C) = F_T - F_L \tag{3.11}$$

3.2. PARTICLE SWARM OPTIMIZATION (PSO) ALGORITHM

Particle Swarm Optimization (PSO) algorithms are crucial in optimization for their simplicity, requiring fewer tuning parameters than some alternatives. They are known for quick convergence, especially in well-behaved optimization problems, and exhibit versatility by handling both continuous and discrete search spaces. The swarm intelligence inherent in PSO, inspired by the collective behavior of social organisms, sets it apart from traditional optimization algorithms. The collaboration among particles, akin to entities in a social group, enables PSO to navigate complex search spaces efficiently. These distinctive features make PSO a valuable tool in optimization tasks, offering a unique approach that complements and, in some cases, outperforms other optimization algorithms.

In PSO, a population of candidate solutions, referred to as particles, iteratively moves through a search space to find the optimal solution. Each particle represents a potential

solution and possesses both a position and velocity. The movement of particles is influenced by both their individual experiences and the experiences of neighboring particles.

The fundamental principles, serving as key strategies that guide the behavior of particles within PSO algorithms, can be categorized into three key principles [104]. The initial principle, Personal Best, dictates that each particle maintains a record of the best location it has discovered thus far as its personal best. This involves the preservation, retention, and documentation of the best value identified up to the present moment. The subsequent principle, Global Best, mandates that particles engage in communication with each other before initiating any movement to update the global best location identified by the entire swarm. This ensures a collective identification and updating of the best position discovered by the entire swarm up to the current instant. The final principle, Current Direction, necessitates that each particle is cognizant of its present direction, which may differ from other particles. This knowledge is crucial as particles leverage it to determine their subsequent location. In the following discussion, a thorough examination of the advantages and disadvantages associated with PSO algorithms will be presented.

One notable advantage is the ease of implementation; PSO is known for its relatively straightforward implementation and comprehensibility, necessitating fewer tuning parameters in comparison to some alternative optimization methods. Another advantage is versatility; PSO exhibits effectiveness in handling both continuous and discrete (binary) search spaces, showcasing its versatility across diverse applications. Additionally, PSO is characterized by quick convergence, particularly in well-behaved optimization problems, owing to its adeptness in balancing exploration and exploitation through velocity updates and particle interactions.

One of the drawbacks is that PSO may face challenges arising from the curse of dimensionality, as the increasing number of dimensions leads to a significantly larger search space, potentially impeding the effectiveness of PSO. Another disadvantage lies in the fact that PSO's performance is contingent on appropriate parameter tuning. Therefore, meticulous parameter selection is essential to fully leverage PSO's potential in various optimization tasks.

3.2.1. THE MATHEMATICAL FRAMEWORK FOR PSO

To enhance comprehension, a visual representation of the Particle Swarm Optimization (PSO) algorithm is provided through a flowchart, as illustrated in Figure 3.4. Commencing with the initialization phase, the PSO algorithm randomly assigns velocity and location to each particle, instigating the exploration of the design space. The number of particles involved in this exploration is determined by the specific optimization problem. Following this, the algorithm evaluates the fitness of each particle by employing an objective function, obtaining values based on this function.

Subsequently, a comparative analysis of the fitness values among individual particles is conducted. If the evaluated values for a particle surpass others, its value is updated; otherwise, the PSO algorithm retains the obtained value and designates it as the Global Best (GBEST) for the entire swarm, essentially assigning the PBEST as GBEST. If the pre-

defined stopping criteria are met at this stage, the optimum solution is deemed found. These stopping criteria may involve a specific number of iterations or achieving a predetermined value, depending on the nature of the problem. If the stopping criteria are not satisfied, the PSO algorithm proceeds to update the velocity and location of the particles. The particles, now possessing updated velocity and location, undergo the evaluation function once again in this iterative process. This iterative process continues until the specified conditions for convergence or a predefined number of iterations are reached.

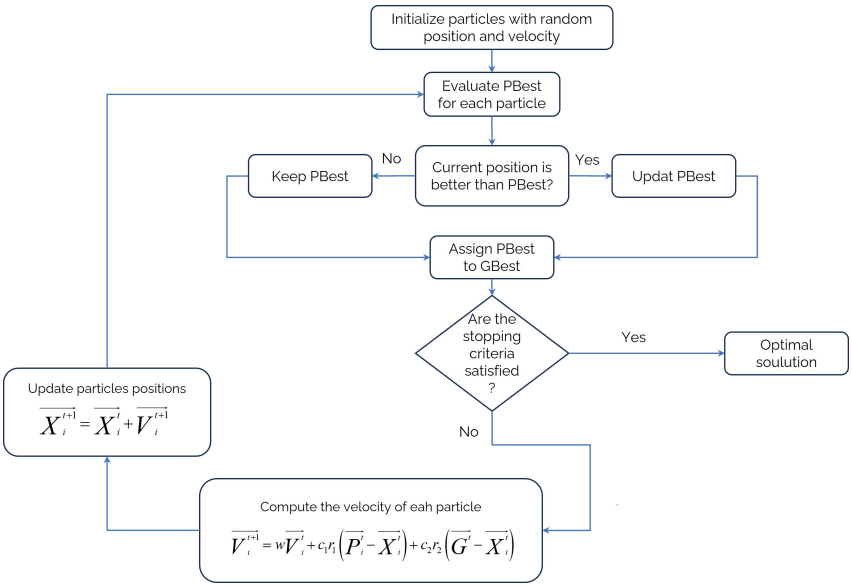

Figure 3.4.: The flowchart provides a visual representation of the PSO algorithm's dynamic of the search space.

In order to update the position of each particle, two vectors are considered: a position vector representing the particle's location in the landscape, and a velocity vector indicating the direction and magnitude of its movement. These vectors are updated in each iteration using the following equations [105]:

$$\overrightarrow{X_i^{t+1}} = \overrightarrow{X_i^t} + \overrightarrow{V_i^{t+1}} \tag{3.12}$$

$$\overrightarrow{V_i^{t+1}} = w\overrightarrow{V_i^t} + c_1 r_1\left(\overrightarrow{P_i^t} - \overrightarrow{X_i^t}\right) + c_2 r_2\left(\overrightarrow{G^t} - \overrightarrow{X_i^t}\right) \tag{3.13}$$

Each particle defines its position with a vector denoted as X_i. To update the position vector, the movement direction and speed are determined using the velocity vector (Equation (3.13)).

The variable t, represents the current iteration, and i denotes the particle number i. The current velocity vector (V_i^t) undergoes scaling by the inertia variable (w). Addition-

ally, c_1 and c_2 pertain to the last two components in the velocity vector. The resultant vector V_i^{t+1} represents the velocity on the next iteration.

The velocity vector comprises three components: current velocity, a tendency towards the personal best (PBEST), and a tendency towards the global best (GBEST). For simplicity, GBEST is referred to as the best solution found by the entire swarm. The determination of the second and third components involves calculating the distance to PBEST $\left(\overrightarrow{P_i^t} - \overrightarrow{X_i^t}\right)$ and GBEST $\left(\overrightarrow{G^t} - \overrightarrow{X_i^t}\right)$.

Each component of the velocity vector has specific terms associated with it. The first term is referred to as the inertia component, as it maintains the current velocity and direction of movement. The second component is known as the cognitive or individual component because each particle considers the distance between its PBEST and its current location, reflecting its individual performance. Conversely, the third component is termed the social component, as particles calculate the distance between their current position and the best position found by the entire swarm (GBEST).

The stochastic nature of the Particle Swarm Optimization (PSO) algorithm arises from the random component introduced into the particle's movement. Instead of moving a fixed distance in each iteration, the particle varies its distance by a factor of r, where r falls within the interval $[0, 1]$ [106]. Indeed, each component is scaled by r to introduce random variations in its impact. This random search component facilitates the exploration of various locations within the design space by the particle.

The influence of cognitive and social components on particle movement can be adjusted by tuning the coefficients c_1 and c_2. The inertia weight regulates the balance between exploration and exploitation. Typically, it is linearly decreased from 0.9 to 0.4 or sometimes even to 0.2. This reduction corresponds to the distance that particles travel each day.

Assessing the influence of control parameters on the performance of the PSO algorithm involves examining the impact of varying values for the inertia weight (w), c_1 and c_2

Setting the inertia weight to zero minimizes exploration, while a value of one maximizes it [107]. Suppose the inertia weight undergoes a linear change from 0.9 to 0.4. The adjustment of the inertia parameter during optimization is recognized for its role in balancing exploration and exploitation, proving to be a valuable mechanism in the quest for the global optimum in real-world problems [107].

Exploring the impact of c_1 and c_2 on the algorithm's performance, two scenarios are considered. In the first scenario ($c_1 = 0$ and $c_2 = 1$), particles focus solely on the best solution found thus far (GBEST), resulting in rapid convergence towards a specific point, which may be a local optimum [108]. In the second scenario ($c_1 = 1$ and $c_2 = 0$), each particle concentrates on exploring a specific portion of the search landscape, eliminating the need for information exchange among particles as they do not require knowledge of GBEST's location [108].

Alternatively, when $c_1 = 0$, and $c_2 = 1$ the exploration is minimized while the exploitation is maximized. Conversely, with $c_1 = 1$ and $c_2 = 0$, exploration is maximized while

exploitation is minimized. Achieving a balance between exploration and exploitation is realized by appropriately tuning c_1 and c_2.

3.2.2. DISCRETE AND BINARY PARTICLE SWARM OPTIMIZATION (DPSO AND BPSO) ALGORITHMS

Discrete Particle Swarm Optimization (DPSO) and Binary Particle Swarm Optimization (BPSO) are variants of the PSO. While traditional PSO is best suited for continuous optimization problems where variables can take any real value within a defined range, DPSO is tailored to handle problems with discrete variables, which can include integer values or binary values. On the other hand, BPSO is specifically designed to handle problems with binary values.

One of the challenges of using DPSO and BPSO is the need to adapt the velocity and position update equations to accommodate the discrete and binary nature of the variables. Depending on the specific problem, different update strategies may be employed, such as integer rounding or binary operations [109].

In Equation (3.12) and Equation (3.13), the update mechanisms for the position and velocity of particles in the PSO algorithm have been addressed. The utilization of velocity to facilitate continuous movement within a search space is demonstrated in Equation (3.13). However, in specific optimization scenarios, particularly those involving discrete and binary variables, particles are required to make discrete or binary choices.

Hence, in this context, particles cease to navigate smoothly through a continuous search space and instead make discrete decisions. The shift from continuous to discrete movement warrants exploration and understanding, particularly in the context of a binary search space within PSO. In essence, the challenge lies in determining the application of velocity vectors when particles are compelled to make binary choices, diverging from the continuous variation of values within a range.

To address this challenge, a transfer function has been introduced to map the velocity vector to a probability vector. This probability vector is then utilized to update the positions of the particles [110]. The transfer function is represented by a Sigmoid function, which can be described as follows:

$$\overrightarrow{X_i^{t+1}} = \begin{cases} 1 & if\ r < T\left(\overrightarrow{V_i^{t+1}}\right) \\ 0 & if\ r \geq T\left(\overrightarrow{V_i^{t+1}}\right) \end{cases} \tag{3.14}$$

$$T\left(\overrightarrow{V_i^{t+1}}\right) = \frac{1}{1 + e^{-\overrightarrow{V_i^{t+1}}}} \tag{3.15}$$

As shown in Figure 3.5, the Sigmoid function yields a value of 0.5 when the velocity is zero. At this juncture, the probability of altering a variable is at its maximum. In contrast, as velocity values approach positive or negative infinity, the Sigmoid transfer function converges to values close to zero or one. As a result, particles are compelled to adopt values of either zero or one for a given parameter.

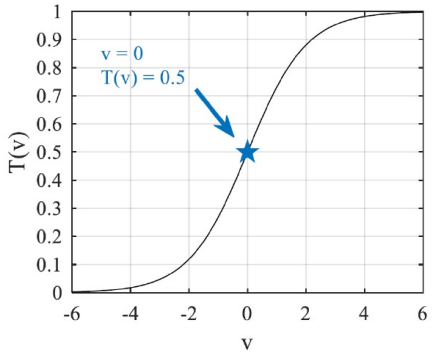

Figure 3.5.: Sigmoid function. It exhibits a distinctive S-shaped curve. The function's characteristic of producing an output of 0.5 when the input is zero makes it valuable for tasks like discrete and binary problems.

3.2.3. CONSTRAINT HANDLING STRATEGIES WITHIN PSO

It is imperative to acknowledge that every search landscape is inherently bounded, and we can employ constraint sets to emulate these boundaries. These constraint sets delineate the upper and lower bounds for all parameters within the optimization problem. Optimization algorithms must incorporate effective mechanisms to reposition solutions that overshoot the boundary, ensuring they reside within the feasible regions of the landscape.

Areas where constraints are violated resemble gaps, which an optimization algorithm should aim to avoid in order to find a global optimum. These constraints effectively divide the search landscape into two categories: feasible and infeasible.

The term "infeasible" indicates that it is possible to obtain a solution that violates the constraints, but this is undesirable and should be circumvented. In cases with a large number of constraints, the landscape may be divided into multiple isolated regions. Consequently, the solutions generated by an optimization algorithm are more likely to fall within the infeasible regions. To address such highly constrained problems, an optimization algorithm should possess the capability to identify these isolated regions and distinguish the promising ones.

Let's consider the minimization of a function described below:

$$f(x_1, x_2, x_3, ..., x_{n-1}, x_n) \tag{3.16}$$

The $x_1, x_2, x_3, ..., x_{n-1}, x_n$ represent the variables involved in the function. The following formulation reveals the presence of two types of constraints: equality and inequality.

$$h_i(x_1, x_2, x_3, ..., x_{n-1}, x_n) = 0, \quad i = 1, 2, 3, ..., p \tag{3.17}$$

$$g_i(x_1, x_2, x_3, ..., x_{n-1}, x_n) \geq 0, \quad i = 1, 2, 3, ..., m \tag{3.18}$$

Equation (3.17) represents an equality constraint, while Equation (3.18) represents an inequality constraint. Additionally, the variable x_i is subject to lower and upper bounds as follows.

$$lb_i \leq x_i \leq ub_i \tag{3.19}$$

When utilizing an optimization algorithm, the handling of these constraints becomes a crucial aspect. Numerous techniques are documented in the literature, with one of the simplest approaches known as the penalty function method [111, 112].

In general terms, a penalty function converts a constrained objective function into an unconstrained one. Incorporating the constraints directly within the objective function is facilitated, eliminating the necessity for modifications to any algorithm. It remains entirely algorithm-independent. A penalty function is defined as follows:

$$f(x) + \sigma P(x) \tag{3.20}$$

where,

$$P(x) = \begin{cases} 0 & if\ x \in S \\ +\infty & otherwise \end{cases} \tag{3.21}$$

σ represents a scalar or constant. It is used to scale the penalty term $P(x)$ in the objective function $f(x) + \sigma P(x)$. The penalty function returns a value of zero if the solution is feasible; in such cases, there is no penalty applied. However, if x is not a feasible solution and violates the constraints, the penalty function penalizes it by assigning a greater objective value than what it should normally return. When a penalty function returns a very large value, it is referred to as a barrier function, and instead of gaps, sudden peaks are encountered.. If a search engine of an optimization algorithm encounters any of these peaks, the algorithm considers it the worst solution due to the very poor objective value. Consequently, this solution is ranked last in the next iteration, and the algorithm attempts to improve it just like any other solutions, without requiring any algorithm modification.

The main drawback of this technique is that it assigns the same penalty value regardless of the number of constraints violated. This uniform penalty may not adequately address the severity of constraint violations in a highly constrained landscape.

3.3. PSO-STEP INTEGRATION

The collaboration between the PSO algorithm and the STEP method is illustrated to highlight the intricacies of their interaction. A flowchart, as depicted in Figure 3.6, has been devised to streamline the description of this collaboration. (For a more detailed version of Figure 3.6, refer to Appendix A.)

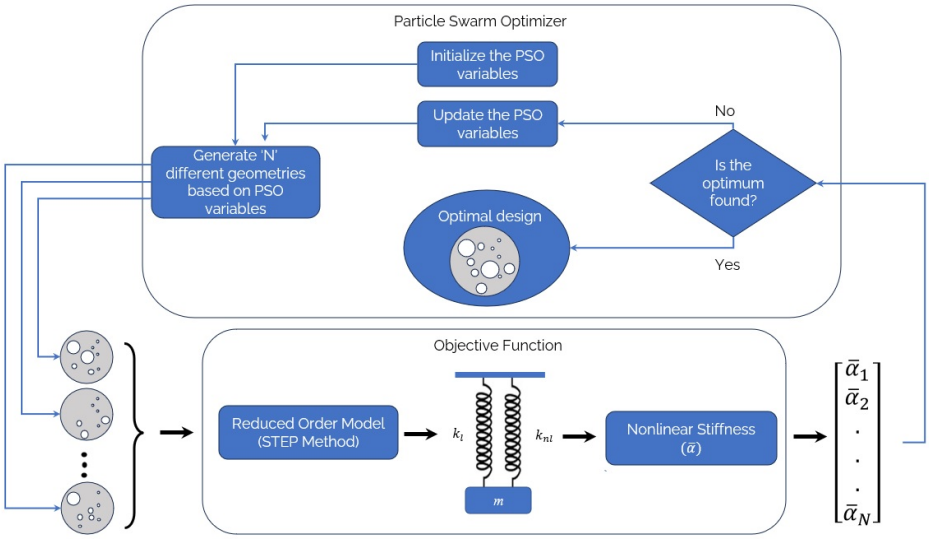

Figure 3.6.: Flowchart of the integrated PSO-STEP algorithm. This procedure includes PSO variable initialization, the generation of different configurations, subsequent calculation of the nonlinear stiffness for each configuration, and finally, finding the optimum solution if all the requirements are satisfied.

Initially, the algorithm initializes its variables based on the specific problem's parameters, setting the stage for the subsequent exploration of the design space. Through the generation of diverse geometries and the assistance of the STEP method, the algorithm calculates the nonlinear stiffness for each configuration, capturing the nuanced interplay of variables in the pursuit of optimal designs. These calculated stiffness values, forming a vector, serve as indicators of the system's performance under various configurations.

The iterative nature of the process is notable, as the algorithm continually refines its search based on the evolving understanding of the design space. The termination criteria, which may include considerations such as the number of particles, iteration count, or specific constraints, determine when the algorithm has converged to an optimal solution or when further exploration is required. This systematic approach, coupled with the adaptability of the PSO algorithm, positions it as a valuable tool for navigating complex design spaces and optimizing configurations to meet specific criteria.

In conclusion, the integrated approach of using the PSO algorithm in conjunction with the STEP method, considering constraints, and employing a penalty function provides a systematic and effective means of determining nonlinear stiffness. This approach significantly contributes to the optimization of our design process.

4

RESULTS AND DISCUSSION

THIS chapter discusses the application of the methods introduced thus far to the design problem defined in Chapter 3. Firstly, the STEP method is incorporated with the COMSOL Finite Element Method (FEM) package, and the validation is performed using reference [35]. The results demonstrate a close agreement between the obtained values for nonlinear stiffness and my incorporated code. Subsequently, a parametric study is conducted to deepen our understanding of the impact of adding circular voids (holes) with varying radii and locations on the nonlinear stiffness of the circular membrane. Finally, the Particle Swarm Optimization (PSO), Discrete Particle Swarm Optimization (DPSO), and Binary Particle Swarm Optimization (BPSO) algorithms are employed alongside the STEP method to determine the optimal design for several special cases.

Proceeding with my analysis, the initial consideration involves a circular membrane with five potential void locations, corresponding to 5 design variables. In this configuration, the radius of the voids remains constant, and only the presence of the voids is subject to variation. Due to the specific nature of the problem definition, the BPSO algorithm is implemented to determine the configuration with the minimum nonlinear stiffness. Following this, the performance of the PSO algorithm is validated within this simplified scenario by incorporating the STEP method to ensure its efficacy.

Expanding the scope of the investigation, the PSO algorithm, encompassing both Binary PSO (BPSO) and Discrete PSO (DPSO) variants, is applied to a more extensive design space. Specifically, the analysis involves problem instances with 30 design variables (representing the number of potential voids locations) using BPSO and 31 design variables (also signifying the number of potential voids locations) with DPSO. Furthermore, the PSO algorithm is implemented for a problem with two design variables, denoted as x and r, representing the location and radius of the voids, respectively. This is carried out to identify configurations with both minimum and maximum nonlinear stiffness.

4.1. STEP METHOD VALIDATION

The validation of the STEP method holds paramount importance in ensuring the accuracy and reliability of the computational results in this thesis. By comparing the outcomes of the STEP method with the established reference [35], the fidelity of the computational

model is intended to be verified. This validation process not only instills confidence in the accuracy of the results but also establishes the credibility of the employed methodology. It ensures that the subsequent analyses and optimization efforts conducted using the STEP method are built upon a robust foundation, enhancing the overall validity and trustworthiness of the research findings.

In reference [35], the authors presented a technique for obtaining Young's modulus of suspended 2D material membranes by analyzing their nonlinear dynamic response. The material properties utilized in their study, along with the circular membrane dimensions they employed, are provided in Table 4.1. They achieved the nonlinear stiffness of $k_{nl} = 1.35 \times 10^{15}\,\mathrm{Nm}^{-3}$.

Table 4.1.: The properties of the material used for a graphene nanodrum, as detailed in reference [35], along with the dimensions of the circular membrane.

Poisson's Ratio (ν)	Young's modulus (E)	Density (ρ)	Radius (R)	Thickness (h)	Prestress (σ)
0.16	594e9[N/m^2]	2330[Kg/m^3]	2.5e-6[m]	5e-9[m]	1e7[N/m^2]

The material properties and dimensions outlined in their paper are utilized to determine the identical nonlinear stiffness that was previously employed in their research for a circular membrane. The results obtained are subsequently presented in Table 4.2. As observed, the obtained results align consistently with those reported in the study by Davidovikj et al. [35]. To enable a thorough examination of relative quantities, the equations are transformed into their dimensionless form. The specifics of the nondimensionalization process are elaborated upon in Appendix B. For reference, the nondimensional nonlinear stiffness is $\overline{k_{nl}} = \frac{k_{nl}h^2}{k_l}$

Table 4.2.: The values obtained for nonlinear stiffness of a circular membrane in both [35] and this thesis are accompanied by the dimensionless form of nonlinear stiffness.

	ref. [35]	This thesis
k_{nl} (Nonlinear Stiffness)	$1.350 \times 10^{15}\,\mathrm{Nm}^{-3}$	$1.3598 \times 10^{15}\,\mathrm{Nm}^{-3}$
$\overline{k_{nl}}$ (Nondimensional Nonlinear Stiffness)	-	1.0091

Please note that from this point forward, when referring to nonlinear stiffness, it is specifically meant in its nondimensional form ($\overline{k_{nl}}$).

Upon validating the STEP results, the subsequent step involves conducting a parametric study to gain a deeper understanding of the impact of adding circular voids on the nonlinear stiffness of a circular membrane.

4.2. PARAMETRIC STUDY

In this section, the objective is to gain a deeper understanding of the effects of adding voids to the circular membrane on its nonlinear stiffness. To achieve this, various voids are introduced with different radii at distinct locations. In conducting a systematic parametric study, an investigation is carried out to discern the impact of location, perforated area (the total surface area deducted from the circular membrane), and the number of voids. It is noteworthy that the perforated area is directly related to the radii of the circular voids. Each parametric study involves fixing two of the parameters while varying the third, enabling the observation of that parameter's specific impact.

4.2.1. PERFORATED AREA VARIATION WITH FIXED VOID LOCATION AND NUMBER

In the initial parametric study, the focus is on a singular void positioned between the center of the circular membrane and the membrane's edge, precisely at coordinates (1.25e-6, 0), with varying radii illustrated in Figure 4.1. This study exclusively involves altering the perforated area (the deducted surface area) of the voids while maintaining constant the location and number of voids. The adjustment in the area deletion corresponds to a modification in the radii of the circular voids. For each configuration, the nonlinear stiffness is determined using the STEP method.

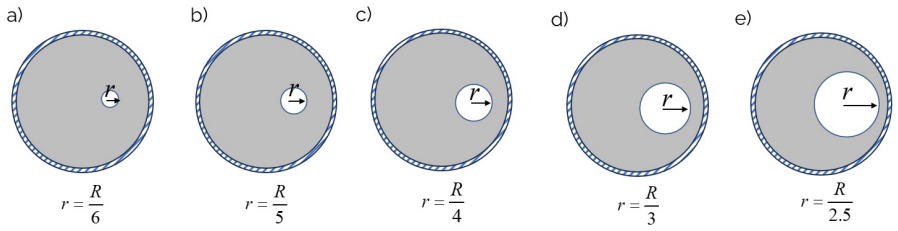

Figure 4.1.: Membrane with void a singular void positioned at the midpoint between the center and the edge with varying radius. As can be seen in Table 4.3, an increase in the void's radius leads to a significant reduction in nonlinear stiffness.

As depicted in Table 4.3, a substantial reduction in nonlinear stiffness emerges when the void is situated between the membrane's center and its edge, and the radius of the void is increased. Put differently, as the void is positioned between the membrane's center and its edge, and the perforated area is increased, the nonlinear stiffness experiences a notable decrease. Notably, in case (**e**), the nonlinear stiffness diminishes by approximately 50 percent compared to a circular membrane without voids.

Table 4.3.: Acquired values of nonlinear stiffness by placing a single void at the midpoint between the center and the edge of the membrane and varying radius as depicted in Figure 4.1.

Cases in Figure 4.1	Nonlinear Stiffness
a)	0.8987
b)	0.8549
c)	0.7804
d)	0.6558
e)	0.5672

4.2.2. SINGLE VOID POSITION VARIATION WITH CONSTANT PERFORATED AREA

In the subsequent scenario, the positions of circular voids are exclusively varied, as detailed in Table 4.4. All circular voids maintain a radius of R/5 and are positioned solely in the $+x$ direction, with a constant y-coordinate of 0. The center of each void is denoted by the coordinates (0,0) for reference. In this configuration, the sole variable subject to alteration is the voids' positions, while the perforated surface area remains consistent across all configurations. The resulting nonlinear stiffness values for each configuration, accompanied by their respective locations (x, y), is provided in Table 4.4.

As indicated in Table 4.4, the relocation of the void towards the edge of the circular membrane correlates with an increase in nonlinear stiffness. It is noteworthy that, in all instances, the movement towards the edge leads to an elevation in nonlinear stiffness. However, this increase does not surpass the nonlinear stiffness observed in a circular membrane without any void.

Table 4.4.: Obtained values of nonlinear stiffness for a membrane with one void positioned solely in the $+x$ direction ($y = 0$), gradually moving towards the edge in various cases.

Different Cases	(x, y)	Nonlinear Stiffness
a)	(0.5e-6, 0)	0.7375
b)	(1e-6, 0)	0.7978
c)	(1.2e-6, 0)	0.8420
d)	(1.5e-6, 0)	0.9133
e)	(1.8e-6, 0)	0.9839

To gain a clearer visualization of the voids' locations on the circular membrane, please refer to Figure 4.2, which illustrates the configurations for all cases.

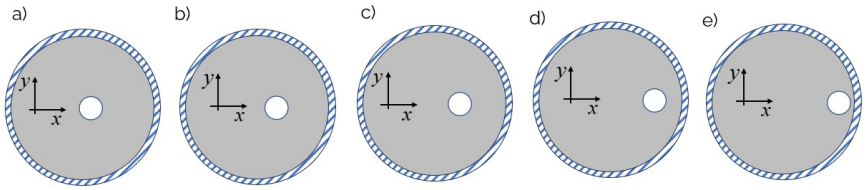

Figure 4.2.: Membrane with one void positioned solely in the $+x$ direction ($y = 0$) for different cases. The nonlinear stiffness tends to increase as the voids approach the membrane's edge, while maintaining a constant perforated area, as depicted in Table 4.4.

4.2.3. VARYING NUMBER OF VOIDS WITH CONSTANT PERFORATED AREA AND VOID LOCATIONS

In another parametric study, the objective is to investigate the effect of increasing the number of voids while maintaining a constant perforated area (see Figure 4.3). In each case presented in Figure 4.3, the number of voids increases while the perforated area remains consistent across all configurations. In case (**a**) presented in Figure 4.3, the radius of the void is R/2.2, and its location is (1.25e-6, 0).

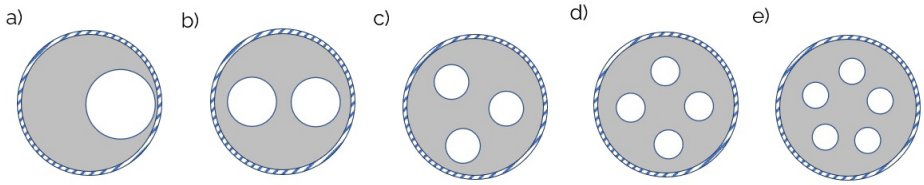

Figure 4.3.: All configurations maintain identical perforated areas. The increase in the number of voids does not lead to a significant alteration in the value of nonlinear stiffness.

For each configuration, the nonlinear stiffness obtained by the STEP method is provided in Table 4.5. As we can see, increasing the number of voids while keeping the perforated area constant does not have a drastic effect on the value of nonlinear stiffness.

Table 4.5.: Obtained values of nonlinear stiffness for all cases as illustrated in Figure 4.3.

Cases in Figure 4.3	Nonlinear Stiffness
a)	0.5167
b)	0.4943
c)	0.5033
d)	0.4989
e)	0.5063

In conclusion, it is crucial to underscore the intricate and interrelated relationship among the location of voids, perforated area, and the number of voids. These three

factors collectively play a pivotal role in shaping the behavior of the circular membrane and its nonlinear stiffness. Their impact on the mechanical properties of the membrane is not isolated but rather interwoven, posing a complex challenge in predicting nonlinear stiffness.

Given the interconnected relation involving void placement, their radii, and the number of voids, it becomes apparent that finding a single configuration for achieving minimum or maximum nonlinear stiffness is a complex challenge, as it does not rely on a single variable but rather the collective interaction of these parameters. Therefore, understanding and optimizing these design parameters is pivotal to achieving the desired mechanical performance of the circular membrane.

In this context, the application of optimization algorithms emerges as a valuable avenue for navigating this intricate design space effectively. Optimization algorithms can serve as a highly effective approach for exploring the optimal design configurations. The Particle Swarm Optimization (PSO) algorithm, in particular, appears to be a valuable tool in this context. The ability of PSO to efficiently navigate complex design spaces and adapt to nonlinear stiffness variations, as observed in this parametric study, can be a promising approach.

4.3. PSO ALGORITHM IMPLEMENTATION AND VALIDATION

In this section, the implementation of the PSO algorithm to discover the optimal solution within a limited design space is targeted, utilizing the material properties and dimensions presented in Table 4.1. The primary focus is on implementing and subsequently validating the PSO algorithm.

The exploration of potential circular void locations within the circular membrane is initiated, as illustrated in Figure 4.4. A grid comprising five points on the circular membrane, denoted by the red-colored voids, has been established. Each of these potential voids has the same radius of R/5. All voids, except for the central one, are positioned at the midpoint between the center and the edge of the circular membrane. For the optimization process, the Binary Particle Swarm Optimization (BPSO) algorithm is employed, selected based on the binary nature inherent in this problem (0 or 1). To clarify, within this circular membrane, a void is represented as 1, and its absence as 0. The void locations and radii remained fixed, with only their presence changing. This leads in a total of $2^5 = 32$ possible configurations (5 design varaibles) in the design space. Each configuration represents a unique combination of void presence or absence at those locations.

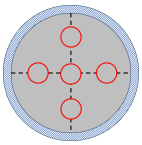

Figure 4.4.: Membrane with a grid of 5 potential void locations. The red-colored voids indicate the possible locations of the voids within the membrane.

Commencing with three particles and conducting ten iterations of the BPSO algorithm, the configuration with the lowest nonlinear stiffness was identified using the BPSO algorithm, as illustrated in the flowchart in Figure 3.6. This configuration is visually represented in Figure 4.5.

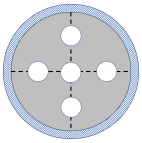

Figure 4.5.: The configuration with minimum nonlinear stiffness found by the BPSO algorithm.

The obtained nonlinear stiffness for each iteration is presented in Table 4.6. The BPSO algorithm identified the minimum nonlinear stiffness in the 9th iteration, which was 0.5933.

Furthermore, it is noteworthy that within my PSO, DPSO, and BPSO codes, code lines have been implemented to display the obtained configurations; for instance, for the obtained configuration, it is shown as [1, 1, 1, 1, 1], where the first number indicates the presence of the void at the center, the second indicates the presence of voids along the +x axis, and the third, fourth, and fifth represent the presence of voids along the +y, -x, and -y axes, respectively. So, this configuration [1, 1, 1, 1, 1] means that there are voids at all five locations.

Table 4.6.: The nonlinear stiffness obtained for each iteration by the BPSO algorithm.

Iteration	1	2	3	4	5	6	7	8	9	10
Nonlinear stiffness	0.9877	0.9877	0.8549	0.8549	0.8549	0.6615	0.6615	0.6615	0.5933	0.5933

The BPSO algorithm has been implemented multiple times, revealing that it identified the optimal configuration in various iterations. This behavior aligns with the intrinsic stochastic nature of particle swarm algorithms, which yield diverse outcomes in each run. Nevertheless, upon conducting multiple runs, a confident conclusion can be drawn that this particular configuration consistently represents the optimal one with the minimum nonlinear stiffness.

To validate the optimality of the solution obtained through BPSO and ascertain its representation of the global optimum, the nonlinear stiffness is computed for every conceivable configuration exclusively through the STEP method. As mentioned earlier, with 5 potential void locations, there are 32 possible configurations. However, as shown in Figure 4.6, some configurations have the same pattern, allowing us to ignore duplicates.

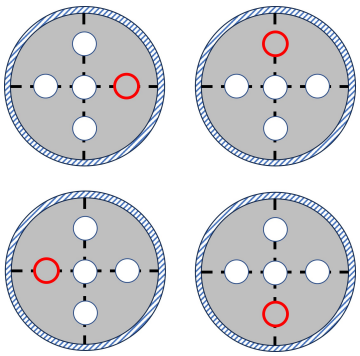

Figure 4.6.: Configurations with the same pattern. Therefore, emphasis is placed on a single representative configuration.

In conclusion, a total of 11 distinct configurations were identified, as depicted in Figure 4.7.

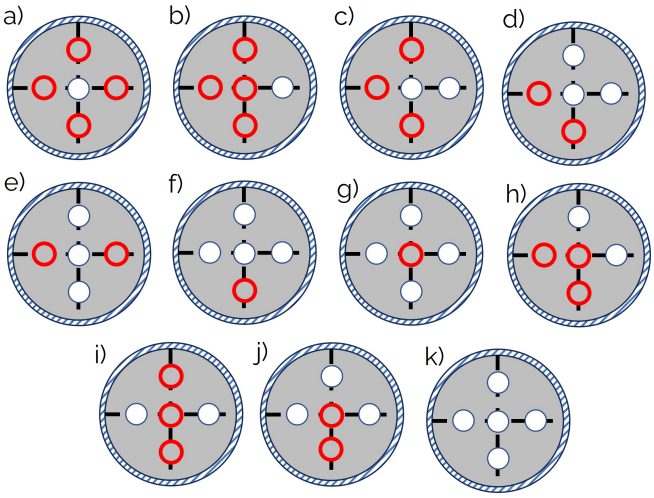

Figure 4.7.: Visualization of 11 distinct configurations out of a total of 32 for calculating nonlinear stiffness using STEP.

The nonlinear stiffness for each configuration in Figure 4.7 is shown in Table 4.7, obtained using the STEP method.

Table 4.7.: Obtained nonlinear stiffness for each configuration in Figure 4.7 using STEP method.

	Nonlinear Stiffness
a)	1.3844
b)	0.8549
c)	0.9877
d)	0.8787
e)	0.7912
f)	0.7011
g)	0.6058
h)	0.7430
i)	0.7471
j)	0.6615
k)	0.5933

The minimum nonlinear stiffness, found using the STEP method, corresponds to case (**k**) and perfectly matches the configuration discovered by the BPSO algorithm, ensuring the algorithm's accuracy.

It is evident that the initial design space is constrained and comparatively straightforward. To address this limitation, steps are taken to expand the design space. To enhance its complexity and comprehensiveness, the decision is made to broaden the design space by investigating five potential void locations along the direction of the membrane radius (R). In total, 30 potential void locations are considered (31 if the membrane center is included).

Additionally, given the potential for experimental validation of the results presented in this thesis, I opt to switch the material to Silicon Nitride (Si_3N_4) and modify the dimensions accordingly. One of our experts in experimental methods has outlined the following parameters and fabrication setup limitations.

The constraints are outlined as follows: The thickness of the circular plate is required to be a minimum of 100 µm. The radius of the circular plate should not surpass 1cm. The distance between the margins of the voids must be at least 500 µm. The minimum allowable radius for the holes is 100 µm.

The properties of the new material and its dimensions are detailed in Table 4.8. It is worth mentioning that the nondimensional nonlinear stiffness for a circular membrane with these material properties and dimensions is 0.9785.

Table 4.8.: The properties of the material used for a Silicon Nitride (Si_3N_4) circular membrane, along with the dimensions of the circular membrane.

Poisson's Ratio (ν)	Young's modulus (E)	Density (ρ)	Radius (R)	Thickness (h)	Prestress (σ)
0.28	170e9[N/m^2]	2329[Kg/m^3]	1e-2[m]	0.1e-3[m]	2e6[N/m^2]

Following calculations based on the distance between the margins of the voids and the minimum radius of the voids, the following potential radii for the voids have been identified: [0.1e-3, 0.2e-3, 0.3e-3, 0.4e-3, 0.5e-3, 0.6e-3, 0.7e-3].

As previously stated, PSO algorithms exhibit stochastic behavior, which can lead to different optimal results in each run. To fortify the robustness of our findings, multiple iterations of the PSO, DPSO, and BPSO algorithms are conducted, and the outcomes from their respective final runs are presented.

4.4. MINIMIZING NONLINEAR STIFFNESS: 30 DESIGN VARIABLES (BPSO)

In this section, consideration is given to 30 potential void locations, excluding one at the center of the circular membrane (see Figure 4.8). All these voids share a common radius of 0.4e-3. Furthermore, the analysis focuses solely on the presence of the voids without alterations in their radius. Given the nature of the problem, the Binary Particle Swarm Optimization (BPSO) algorithm is implemented for this specific case. As previously elucidated regarding the BPSO algorithm, the approach is confined to binary design parameters: 0 denotes the absence of a void, and 1 signifies the presence of a void. Consequently, the design space encompasses 2^{30} possible configurations. A pivotal constraint is imposed, wherein the final configuration, following the addition of voids, must not exceed the removal of more than 30 percent of the membrane's surface area. It is noteworthy that a penalty function is employed as an effective strategy for constraint management, obviating the necessity for extensive modifications to the algorithm.

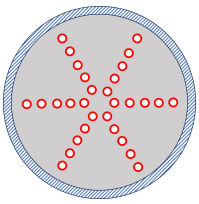

Figure 4.8.: Membrane with all possible void locations except the center, analyzed using the BPSO algorithm to identify the configuration with the minimum nonlinear stiffness.

The BPSO algorithm is employed with 30 particles over 10,000 iterations to ascertain

the optimal configuration that minimizes nonlinear stiffness. Figure 4.9 illustrates the optimization process conducted by the BPSO algorithm, presenting the nonlinear stiffness values obtained for each iteration. It is noteworthy that the nonlinear stiffness for iteration 0 corresponds to a configuration with no voids in the circular membrane. The black dots in Figure 4.9 depict the nonlinear stiffness values obtained by each particle, with the red dots indicating the best value discovered by the entire swarm thus far. The green dot in the figure highlights the iteration during which the BPSO algorithm identified the minimum nonlinear stiffness.

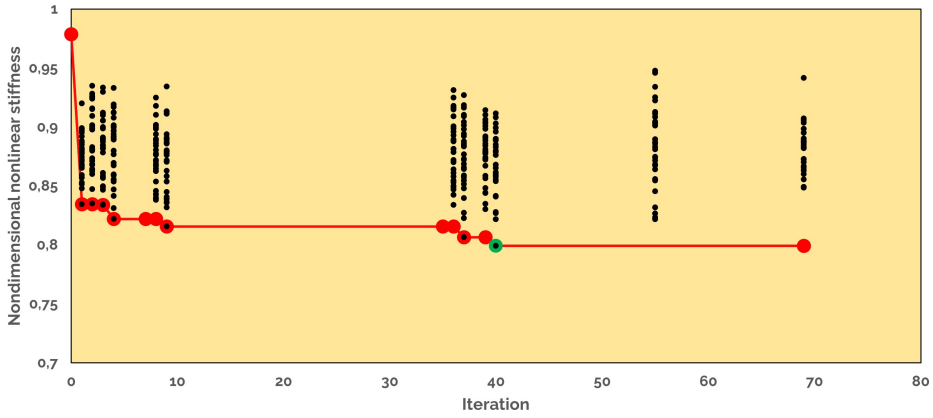

Figure 4.9.: Overview of the BPSO algorithm process. The minimum nonlinear stiffness was found in the iteration 40th, exhibiting a nonlinear stiffness value of 0.7989.

Figure 4.10 displays configurations discovered by BPSO during specific iterations. As illustrated, the configuration in the 40th iteration has the minimum nonlinear stiffness.

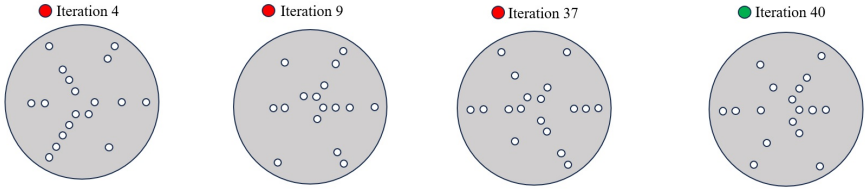

Figure 4.10.: The evolutionary process of finding the optimal configuration with the minimum nonlinear stiffness using the BPSO algorithm.

To facilitate a deeper comprehension of changes in nonlinear stiffness, the nonlinear stiffness values for specific iterations are presented in Table 4.9. As observed, the minimum nonlinear stiffness is found in the 40th iteration. Additionally, the final optimum nonlinear stiffness, displayed in Table 4.9, exhibits a nonlinear stiffness of 0.7989, representing a remarkable 20 percent reduction in nonlinear stiffness. The values found by each particle in iterations 1, 37, and 40 are provided in Appendix C.

Table 4.9.: The nonlinear stiffness obtained for a specific iteration by the BPSO algorithm.

Iteration	0	1	3	4	9	37	40	45	50	66
Nonlinear stiffness	0.9785	0.8343	0.8337	0.8219	0.8156	0.8065	0.7989	0.7989	0.7989	0.7989

4.5. MINIMIZING NONLINEAR STIFFNESS: 31 DESIGN VARIABLES (DPSO)

In this segment, consideration is given to 31 potential void locations, including one at the center of the circular membrane (see Figure 4.11). These voids can have different radii selected from the range [0, 0.1e-3, 0.2e-3, 0.3e-3, 0.4e-3, 0.5e-3, 0.6e-3, 0.7e-3]. In this case, the design variable pertains to the radius of the voids, which can assume discrete values.

Due to the utilization of discrete values for the radii of the voids, the Discrete Particle Swarm Optimization (DPSO) algorithm is implemented for this particular problem. It is important to note that when the radius is set to 0, it signifies the absence of a void. The problem was subject to constraints to ensure the final configuration, post-void addition, did not result in the removal of more than 30 percent of the membrane's surface area. Furthermore, constraints were imposed to prevent interference among the added voids, mandating the maintenance of specified margins between them, as previously delineated, in accordance with experimental limitations.

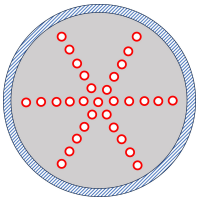

Figure 4.11.: Membrane with all possible void locations including the center, analyzed using the DPSO algorithm to identify the configuration with the minimum nonlinear stiffness

In Figure 4.12, a visual representation of the optimization process conducted by the DPSO algorithm is presented, showcasing the nonlinear stiffness values obtained during each iteration. The 12th iteration yielded the minimum nonlinear stiffness, with a value of 0.7610.

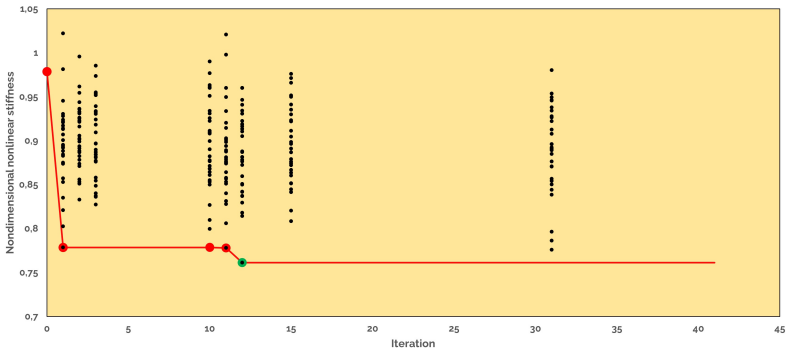

Figure 4.12.: Overview of the DPSO algorithm process. The minimum nonlinear stiffness was found in the iteration 12th, exhibiting a nonlinear stiffness value of 0.7610.

Figure 4.13 showcases three configurations identified by the BPSO algorithm at distinct iterations. Notably, the configuration attained in the 12th iteration exhibits the lowest nonlinear stiffness.

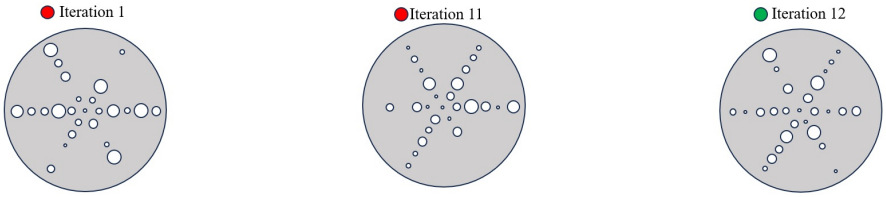

Figure 4.13.: The evolutionary procedure involves identifying the optimal configuration with the lowest nonlinear stiffness through the implementation of DPSO.

A more detailed representation of the configuration with the minimum nonlinear stiffness is shown in Figure 4.14. Specific numbers have been assigned to each void, and their corresponding radii are presented in Table 4.10.

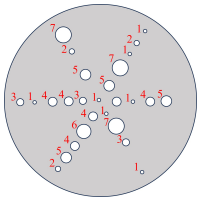

Figure 4.14.: Designated number corresponding to each void for 12th iteration in Figure 4.13. The radius related to each void is provided in Table 4.10.

Table 4.10.: The radius value for each designated void in Figure 4.14.

Labeled Void Number	1	2	3	4	5	6	7
Radius [m]	0.1e-3	0.2e-3	0.3e-3	0.4e-3	0.5e-3	0.6e-3	0.7e-3

Table 4.11 clearly indicates that the DPSO algorithm achieved convergence, reaching the optimal design during the 12th iteration. The ultimate optimal nonlinear stiffness recorded a value of 0.7610, representing a significant 20 percent reduction in nonlinear stiffness. Details of the results obtained by individual particles in the first, 11th, and 12th iterations are provided in Appendix C.

Table 4.11.: The nonlinear stiffness value obtained for specific iterations by the DPSO algorithm.

Iteration	0	1	11	12	15	22	30	40
Nonlinear stiffness	0.9785	0.7785	0.7780	0.7610	0.7610	0.7610	0.7610	0.7610

4.6. OPTIMIZING NONLINEAR STIFFNESS: 2 DESIGN VARIABLES (PSO)

In this scenario, a case is considered with only one void, positioned exclusively along the $+x$ (with its y-coordinate always set to 0). The $+x$-coordinate of this void is allowed to vary within the range of 0 to R. Furthermore, the radius of this void can assume values within the range of [0.1e-3 to 7e-3]. This scenario involves two design variables: x and r (the void's radius). Considering the potential to discover an optimal design within this extensive design space and recognizing the continuous nature of the design variables, the Particle Swarm Optimization (PSO) algorithm is implemented. The objective is to identify two configurations: one that minimizes nonlinear stiffness and another that maximizes it.

4.6.1. MINIMIZING NONLINEAR STIFFNESS

Presently, the objective is to utilize the PSO algorithm to identify the configuration that results in the lowest nonlinear stiffness. The constraint for this problem dictates that the created voids must remain within the boundaries of the circular membrane, maintaining a specified margin from the membrane's edge.

In Figure 4.15, a graphical representation illustrating the optimization process conducted by the PSO algorithm is provided. This visualization showcases the nonlinear stiffness values obtained at each iteration. The PSO algorithm successfully identified

the configuration with the minimum nonlinear stiffness by the 29th iteration. The minimum nonlinear stiffness obtained by the PSO algorithm decreased by approximately 70 percent compared to a circular membrane with no void.

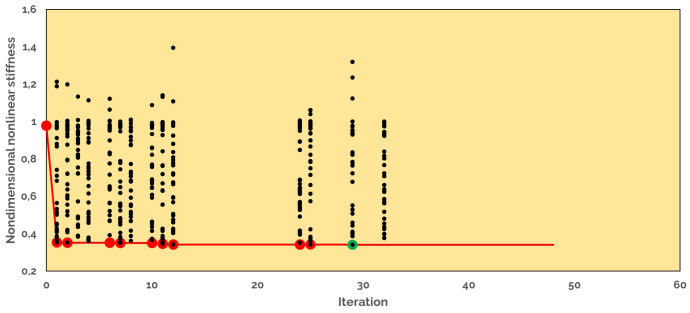

Figure 4.15.: Overview of the PSO algorithm process for finding the minimum nonlinear stiffness. The minimum nonlinear stiffness was found in the iteration 29th, exhibiting a nonlinear stiffness value of 0.3404.

In Figure 4.16, we can observe the configurations obtained during specific iterations aimed at minimizing nonlinear stiffness. It is clear that larger voids positioned nearer to the edge of the circular membrane lead to reduced nonlinear stiffness.

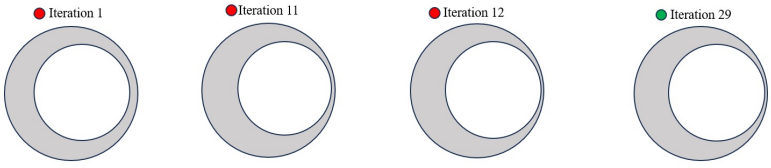

Figure 4.16.: Configurations found by the PSO algorithm for minimizing nonlinear stiffness.

However, discerning the differences in void locations and radii might not be straightforward from Figure 4.16 alone. For a more comprehensive perspective, a dedicated table, labeled as Table 4.12, has been included, presenting the x-locations and radii of each configuration depicted in Figure 4.16.

Table 4.12.: Detailed x location and r values for each configuration in Figure 4.16.

Iteration	Nonlinear Stiffness	x [m]	r [m]
1	0.35315	0.0015607	0.0069445
11	0.34661	0.0025791	0.0068121
12	0.34286	0.0025532	0.0068964
29	0.34047	0.0029295	0.0069467

The PSO algorithm has generated values, which are recorded in Table 4.13, for specific iterations aimed at minimizing nonlinear stiffness.The outcomes achieved by individual particles during the first, 25th, and 129th iterations have been recorded in Appendix C. Furthermore, the x-location and radius (r) of each particle found in the first iteration are provided in Appendix C.

Table 4.13.: The nonlinear stiffness value obtained for specific iterations by the PSO algorithm to find the minimum nonlinear stiffness.

Iteration	0	1	2	12	25	29	34	45
Nonlinear stiffness	0.9785	0.35315	0.3522	0.3428	0.3424	0.3404	0.3404	0.3404

4.6.2. MAXIMIZING NONLINEAR STIFFNESS

In this section, the focus shifts to implementing the PSO algorithm to pinpoint the configuration with the maximum nonlinear stiffness. In Figure 4.17, we can observe the optimization process of the PSO algorithm as it seeks the configuration with the highest nonlinear stiffness. It is evident that the algorithm reaches the optimal design in iteration 17th.

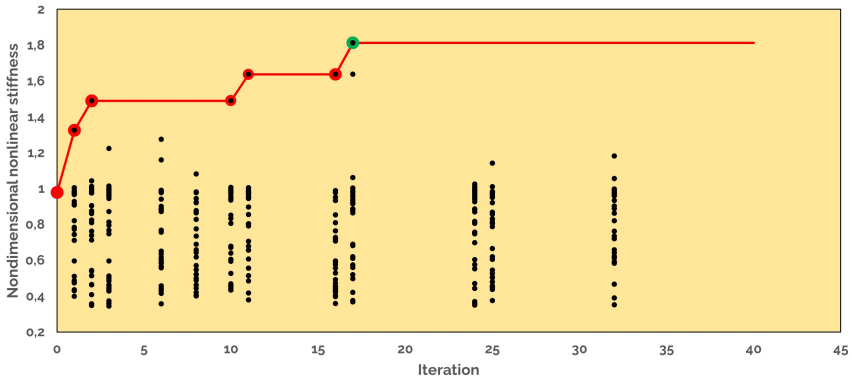

Figure 4.17.: Overview of the PSO algorithm process for finding the maximum nonlinear stiffness. The maximum nonlinear stiffness was found in the 17th iteration, exhibiting a nonlinear stiffness value of 1.8133.

The configurations obtained for these specific iterations, along with the optimal configuration with the maximum nonlinear stiffness, are illustrated in Figure 4.18.

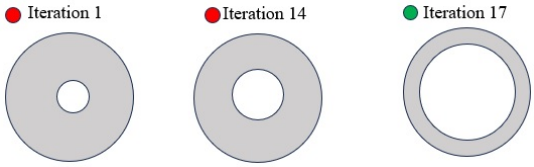

Figure 4.18.: Configurations found by the PSO algorithm for maximizing nonlinear stiffness.

Since the differences between the obtained configurations may not be readily discernible, we have provided detailed information for the x-location and radius (r) of each configuration in Table 4.14.

Table 4.14.: Detailed x location and r values for each configuration in Figure 4.18.

Iteration	Nonlinear Stiffness	x [m]	r [m]
1	1.3257	3.171e-05	0.0022221
14	1.6374	2.4311e-06	0.004897
17	1.8133	0	0.007

Table 4.15 displays the values discovered by the PSO algorithm during certain iterations focused on maximizing nonlinear stiffness. The outcomes derived by individual particles during the first, 14th, and 17th iterations have been recorded in Appendix C. Moreover, Appendix C contains information on the x-coordinate and radius for each particle identified during the initial iteration.

Table 4.15.: The nonlinear stiffness value obtained for specific iteratiosn by the DPSO algorithm to find the maximum nonlinear stiffness..

Iteration	0	1	2	3	7	14	17	40
Nonlinear stiffness	0.9785	1.3257	1.4896	1.4896	1.4896	1.6374	1.8133	1.8133

The outcomes derived from the Particle Swarm Optimization (PSO) algorithm, designed to minimize and maximize nonlinear stiffness, align remarkably well with the results obtained through the comprehensive parametric study conducted. This agreement emphasizes the effectiveness and reliability of the PSO algorithm in exploring the intricate design space.

In essence, the success of PSO algorithms in finding optimal solutions is underscored by the intricate interplay between the location, radii, and number of voids, all of which directly influence the deducted surface area. The complex relationships among these parameters make the PSO algorithms a promising avenue for navigating the design space and uncovering optimal solutions with enhanced efficiency and precision.

Moreover, the PSO optimization reveals that a mere random increase in the number of voids does not significantly alter the nonlinear stiffness. This suggests that the critical factors influencing the nonlinear stiffness are primarily associated with the specific locations of the voids and the resulting deducted surface area. The findings emphasize the importance of these factors in determining the substantial changes in nonlinear stiffness.

5

CONCLUSION

In this study, the potential of design optimization in fine-tuning the nonlinear stiffness of a circular membrane was illustrated. This approach enables a systematic assessment of a wide range of design configurations, pinpointing the optimal design through the utilization of PSO algorithms, including DPSO and BPSO.

The findings of this research carry important implications for the design of high- performance structures with specific stiffness requirements. By utilizing PSO algorithms, including DPSO and BPSO, for design optimization, a significant reduction in time and cost associated with traditional trial-and-error approaches can be achieved. Furthermore, this study provides valuable insights into the fundamental mechanisms governing the influence of circular voids on the nonlinear stiffness of a circular membrane. The investigations conducted within this thesis shed light on the interconnected relationship among void location, radii, and the number of voids, all intricately linked to the alteration of the circular membrane's surface area. These discoveries have significant potential to enhance the development of more accurate models and design guidelines.

Moreover, the approach outlined in this thesis introduces a pioneering methodology for the implementation of PSO algorithms in design optimization, marking a significant advancement in this field. This methodology proves valuable not only for the design optimization of circular membranes but also holds promise for application in other, more complex structures, such as beams or plates.

In summary, the application of particle swarm optimization algorithms emerges as a promising tool for optimizing design exploration and revealing the fundamental principles governing complex materials and structural behavior. Additionally, this thesis endeavors to emphasize the capability of the PSO algorithm in streamlining the design process. It is hoped that these findings will act as a catalyst for further research in this captivating domain, playing a pivotal role in advancing the development of more efficient and effective design methodologies.

For future work, it is proposed to leverage machine learning as a powerful tool for exploring the design space, providing a broader understanding of the impact of void locations and their radii. While machine learning (ML) has found widespread application in various fields, its adoption in engineering science is still in its nascent stages. Employ-

ing ML models to discern patterns and relationships within the data enables engineers to develop optimized designs that surpass the performance of initial designs. As data availability increases and more advanced ML techniques evolve, there is an opportunity to unlock even greater efficiencies in the design process. Additionally, exploring experimental validation of the obtained results could offer further avenues for investigation.

REFERENCES

[1] J. F. Rhoads, S. W. Shaw and K. L. Turner. 'Nonlinear dynamics and its applications in micro-and nanoresonators'. In: (2010). DOI: 10.1115/1.4001333.

[2] S. E. Lyshevski. *Nano-and micro-electromechanical systems: fundamentals of nano- and microengineering*. CRC press, 2018.

[3] K. Muldoon, Y. Song, Z. Ahmad, X. Chen and M.-W. Chang. 'High Precision 3D Printing for Micro to Nano Scale Biomedical and Electronic Devices'. In: *Micromachines* 13.4 (2022), p. 642. DOI: 10.3390/mi13040642.

[4] S. Zhang, X. Xu, T. Lin and P. He. 'Recent advances in nano-materials for packaging of electronic devices'. In: *Journal of Materials Science: Materials in Electronics* 30 (2019), pp. 13855–13868. DOI: 10.1007/s10854-019-01790-3.

[5] M. Packianather, C. Le, D. T. Pham and H. Q. Le. 'Advanced micro and nano manufacturing technologies used in medical domain'. In: *6th International Conference on the Development of Biomedical Engineering in Vietnam (BME6) 6*. Springer. 2018, pp. 637–642. DOI: 10.1007/978-981-10-4361-1_109.

[6] A. A. Abdellatif, H. A. Mohammed, R. A. Khan, V. Singh, A. Bouazzaoui, M. Yusuf, N. Akhtar, M. Khan, A. Al-Subaiyel, S. A. Mohammed *et al.* 'Nano-scale delivery: A comprehensive review of nano-structured devices, preparative techniques, site-specificity designs, biomedical applications, commercial products, and references to safety, cellular uptake, and organ toxicity'. In: *Nanotechnology Reviews* 10.1 (2021), pp. 1493–1559. DOI: 10.1515/ntrev-2021-0096.

[7] D. Puglia, M. A. S. Al-Maadeed, J. M. Kenny, S. Thomas *et al.* 'Elastomer/thermoplastic modified epoxy nanocomposites: The hybrid effect of microand nanoscale'. In: *Materials Science and Engineering: R: Reports* 116 (2017), pp. 1–29. DOI: 10.1016/j.mser.2017.03.001.

[8] M. Liu and X. Li. 'Mechanical properties measurement of materials and devices at micro-and nano-scale by optical methods: A review'. In: *Optics and Lasers in Engineering* 150 (2022), p. 106853. DOI: 10.1016/j.optlaseng.2021.106853.

[9] S. T. Smith and R. M. Seugling. 'Sensor and actuator considerations for precision, small machines'. In: *Precision engineering* 30.3 (2006), pp. 245–264. DOI: 10.1016/j.precisioneng.2005.10.003.

[10] H. Tzou, H.-J. Lee and S. Arnold. 'Smart materials, precision sensors/actuators, smart structures, and structronic systems'. In: *Mechanics of Advanced Materials and Structures* 11.4-5 (2004), pp. 367–393. DOI: 10.1080/15376490490451552.

[11] O. Rioul and M. Vetterli. 'Wavelets and signal processing'. In: *IEEE signal processing magazine* 8.4 (1991), pp. 14–38. DOI: 10.1109/79.91217.

[12] C. T.-C. Nguyen. 'Transceiver front-end architectures using vibrating micromechanical signal processors'. In: *RF Technologies for Low Power Wireless Communications* (2001), pp. 411–461. DOI: 10.1002/0471221643.ch12.

[13] K. J. Hemker and W. N. Sharpe Jr. 'Microscale characterization of mechanical properties'. In: *Annu. Rev. Mater. Res.* 37 (2007), pp. 93–126. DOI: 10.1146/annurev.matsci.36.062705.134551.

[14] A. Tyagi, K. M. Tripathi and R. K. Gupta. 'Recent progress in micro-scale energy storage devices and future aspects'. In: *Journal of Materials Chemistry A* 3.45 (2015), pp. 22507–22541. DOI: 10.1039/C5TA05666G.

[15] L. Zimmermann, J. P. Ebersohl, F. Le Hung, J. Berry, F. Baillieu, P. Rey, B. Diem, S. Renard and P. Caillat. 'Airbag application: a microsystem including a silicon capacitive accelerometer, CMOS switched capacitor electronics and true self-test capability'. In: *Sensors and Actuators A: Physical* 46.1-3 (1995), pp. 190–195. DOI: 10.1016/0924-4247(94)00888-0.

[16] P. Vinay, C. Vamsi, M. Hemanth, A. Saiteja, M. A. Ali and P. A. Kumar. 'Design and simulation of MEMS based accelerometer for crash detection and air bags deployment in automobiles'. In: *International Journal of Mechanical Engineering and Technology* 8.4 (2017), pp. 424–434.

[17] C. D. Meinhart and H. Zhang. 'The flow structure inside a microfabricated inkjet printhead'. In: *Journal of microelectromechanical systems* 9.1 (2000), pp. 67–75. DOI: 10.1109/84.825779.

[18] Y. H. Yun, J. D. Kim, B. K. Lee, Y. W. Cho and H. Y. Lee. 'Polymer inkjet printing: Construction of three-dimensional structures at micro-scale by repeated lamination'. In: *Macromolecular research* 17 (2009), pp. 197–202. DOI: 10.1007/BF03218679.

[19] V. M. Passaro, A. Cuccovillo, L. Vaiani, M. De Carlo and C. E. Campanella. 'Gyroscope technology and applications: A review in the industrial perspective'. In: *Sensors* 17.10 (2017), p. 2284. DOI: 10.3390/s17102284.

[20] K. Liu, W. Zhang, W. Chen, K. Li, F. Dai, F. Cui, X. Wu, G. Ma and Q. Xiao. 'The development of micro-gyroscope technology'. In: *Journal of Micromechanics and Microengineering* 19.11 (2009), p. 113001. DOI: 10.1088/0960-1317/19/11/113001.

[21] D. K. Miu and Y.-C. Tai. 'Silicon microstructures and microactuators for compact computer disk drives'. In: *IEEE Control Systems Magazine* 14.6 (1994), pp. 52–57. DOI: 10.1109/37.334415.

[22] L. J. Hornbeck. 'The DMDTM projection display chip: a MEMS-based technology'. In: *Mrs Bulletin* 26.4 (2001), pp. 325–327. DOI: 10.1557/mrs2001.72.

[23] N. Yu, Y. Liu, B. Ji, S. Wang, Y. Chen, T. Sun, J. Zhang and B. Yang. 'High-sensitivity microliter blood pressure sensors based on patterned micro-nanostructure arrays'. In: *Lab on a Chip* 20.9 (2020), pp. 1554–1561. DOI: 10.1039/D0LC00063A.

[24] T.-W. Yeow, K. E. Law and A. Goldenberg. 'MEMS optical switches'. In: *IEEE Communications magazine* 39.11 (2001), pp. 158–163. DOI: 10.1109/35.965375.

[25] D. C. Roberts, H. Li, J. L. Steyn, O. Yaglioglu, S. M. Spearing, M. A. Schmidt and N. W. Hagood. 'A piezoelectric microvalve for compact high-frequency, high-differential pressure hydraulic micropumping systems'. In: *Journal of Microelectromechanical Systems* 12.1 (2003), pp. 81–92. DOI: 10.1109/JMEMS.2002.807471.

[26] M. Unal, Y. Alapan, H. Jia, A. G. Varga, K. Angelino, M. Aslan, I. Sayin, C. Han, Y. Jiang, Z. Zhang *et al.* 'Micro and nano-scale technologies for cell mechanics'. In: *Nanobiomedicine* 1.Godite 2014 (2014), pp. 1–5.

[27] Y. Shao and J. Fu. 'Integrated micro/nanoengineered functional biomaterials for cell mechanics and mechanobiology: a materials perspective'. In: *Advanced Materials* 26.10 (2014), pp. 1494–1533. DOI: 10.1002/adma.201304431.

[28] K. V. Selvan and M. S. M. Ali. 'Micro-scale energy harvesting devices: Review of methodological performances in the last decade'. In: *Renewable and Sustainable Energy Reviews* 54 (2016), pp. 1035–1047. DOI: 10.1016/j.rser.2015.10.046.

[29] G. Liu, W. Jin and N. Xu. 'Two-dimensional-material membranes: a new family of high-performance separation membranes'. In: *Angewandte Chemie International Edition* 55.43 (2016), pp. 13384–13397. DOI: 10.1002/anie.201600438.

[30] A. Gugliuzza, A. Politano and E. Drioli. 'The advent of graphene and other two-dimensional materials in membrane science and technology'. In: *Current opinion in chemical engineering* 16 (2017), pp. 78–85. DOI: 10.1016/j.coche.2017.03.003.

[31] H. P. Kumar and M. A. Xavior. 'Graphene reinforced metal matrix composite (GRMMC): a review'. In: *Procedia Engineering* 97 (2014), pp. 1033–1040. DOI: 10.1016/j.proeng.2014.12.381.

[32] A. Nag, A. Mitra and S. C. Mukhopadhyay. 'Graphene and its sensor-based applications: A review'. In: *Sensors and Actuators A: physical* 270 (2018), pp. 177–194. DOI: 10.1016/j.sna.2017.12.028.

[33] J. Zhu, D. Yang, Z. Yin, Q. Yan and H. Zhang. 'Graphene and graphene-based materials for energy storage applications'. In: *Small* 10.17 (2014), pp. 3480–3498. DOI: 10.1002/smll.201303202.

[34] I. E. Roso, A. Japaridze, P. G. Steeneken, C. Dekker and F. Alijani. 'Probing nanomotion of single bacteria with graphene drums'. In: *Nature Nanotechnology* 17.6 (2022), pp. 637–642. DOI: 10.1038/s41565-022-01111-6.

[35] D. Davidovikj, F. Alijani, S. J. Cartamil-Bueno, H. S. van der Zant, M. Amabili and P. G. Steeneken. 'Nonlinear dynamic characterization of two-dimensional materials'. In: *Nature Communications* 8.1 (2017), p. 1253. DOI: 10.1038/s41467-017-01351-4.

[36] R. Devaney. *An introduction to chaotic dynamical systems*. CRC press, 2018. DOI: 10.4324/9780429502309.

[37] E. Ott. 'Strange attractors and chaotic motions of dynamical systems'. In: *Reviews of Modern Physics* 53.4 (1981), p. 655. DOI: 10.1103/RevModPhys.53.655.

[38] A. C. Luo and R. P. Han. 'The resonance theory for stochastic layers in nonlinear dynamic systems'. In: *Chaos, Solitons & Fractals* 12.13 (2001), pp. 2493–2508. DOI: 10.1016/S0960-0779(00)00225-3.

[39] T. Fossen and H. Nijmeijer. *Parametric resonance in dynamical systems*. Springer Science & Business Media, 2011.

[40] A. N. Michel, L. Hou and D. Liu. *Stability of dynamical systems*. Springer, 2008.

[41] H. Leipholz. *Stability theory: an introduction to the stability of dynamic systems and rigid bodies*. Springer-Verlag, 2013.

[42] D. A. Marshall, L. Burgos-Liz, M. J. IJzerman, N. D. Osgood, W. V. Padula, M. K. Higashi, P. K. Wong, K. S. Pasupathy and W. Crown. 'Applying dynamic simulation modeling methods in health care delivery researchthe SIMULATE checklist: report of the ISPOR simulation modeling emerging good practices task force'. In: *Value in health* 18.1 (2015), pp. 5–16. DOI: 10.1016/j.jval.2014.12.001.

[43] M. Cartmell, S. Ziegler, R. Khanin and D. Forehand. 'Multiple scales analyses of the dynamics of weakly nonlinear mechanical systems'. In: *Appl. Mech. Rev.* 56.5 (2003), pp. 455–492. DOI: 10.1115/1.1581884.

[44] H. N. Ali and W. Lacarbonara. 'On the Discretization of Spatially Continuous Systems with Quadratic and Cubic Nonlinearities (Special Issue on Nonlinear Dynamics)'. In: *JSME International Journal Series C Mechanical Systems, Machine Elements and Manufacturing* 41.3 (1998), pp. 510–531. DOI: 10.1299/jsmec.41.510.

[45] C.-Y. Chia. 'Geometrically nonlinear behavior of composite plates: a review'. In: (1988). DOI: 10.1115/1.3151873.

[46] M. Tlidi and M. G. Clerc. 'Nonlinear dynamics: Materials, theory and experiments'. In: *Springer Proceedings in Physics* 173 (2016).

[47] M. Orlik. 'Self-organization in nonlinear dynamical systems and its relation to the materials science'. In: *Journal of Solid State Electrochemistry* 13 (2009), pp. 245–261. DOI: 10.1007/s10008-008-0554-y.

[48] C.-Q. Huang, J. Deng, S.-X. Wang and L.-l. Liu. 'A physical-based constitutive model to describe the strain-hardening and dynamic recovery behaviors of 5754 aluminum alloy'. In: *Materials Science and Engineering: A* 699 (2017), pp. 106–113. DOI: 10.1016/j.msea.2017.04.086.

[49] J.-L. Ha, J.-R. Chang and R.-F. Fung. 'Nonlinear dynamic behavior of a moving viscoelastic string undergoing three-dimensional vibration'. In: *Chaos, Solitons & Fractals* 33.4 (2007), pp. 1117–1134. DOI: 10.1016/j.chaos.2006.01.069.

[50] K. G. Holt, R. O. Wagenaar and E. Saltzman. 'A dynamic systems: constraints approach to rehabilitation'. In: *Brazilian Journal of Physical Therapy* 14 (2010), pp. 446–463. DOI: 10.1590/S1413-35552010000600002.

[51] J. G. Papastavridis and K. Yagasaki. 'Analytical mechanics: a comprehensive treatise on the dynamics of constrained systems; for engineers, physicists, and mathematicians'. In: *Appl. Mech. Rev.* 56.2 (2003), B22–B22. DOI: 10.1115/1.1553436.

[52] C. H. Jenkins and J. W. Leonard. 'Nonlinear dynamic response of membranes: state of the art'. In: (1991). DOI: 10.1115/1.3119506.

[53] A. Sharma, N. Upadhyay, P. K. Kankar and M. Amarnath. 'Nonlinear dynamic investigations on rolling element bearings: A review'. In: *Advances in Mechanical Engineering* 10.3 (2018), p. 1687814018764148. DOI: 10.1177/1687814018764148.

[54] P. Qiao and W. K. Binienda. 'Impact behavior and high-energy absorbing materials'. In: *Journal of Aerospace Engineering* 21.4 (2008), pp. 195–196. DOI: 10.1061/(ASCE)0893-1321(2008)21:4(195).

[55] K. Worden, G. R. Tomlinson and K. Yagasaki. 'Nonlinearity in structural dynamics: detection, identification and modeling'. In: *Appl. Mech. Rev.* 55.2 (2002), B26–B27. DOI: 10.1115/1.1451161.

[56] G. Rega, V. Settimi and S. Lenci. 'Chaos in one-dimensional structural mechanics'. In: *Nonlinear Dynamics* 102.2 (2020), pp. 785–834. DOI: 10.1007/s11071-020-05849-3.

[57] G. Rega and V. Settimi. 'Global dynamics perspective on macro-to nano-mechanics'. In: *Nonlinear Dynamics* 103.2 (2021), pp. 1259–1303. DOI: 10.1007/s11071-020-06198-x.

[58] P. Balaji and K. Karthik SelvaKumar. 'Applications of nonlinearity in passive vibration control: a review'. In: *Journal of Vibration Engineering & Technologies* 9 (2021), pp. 183–213. DOI: 10.1007/s42417-020-00216-3.

[59] M. F. Daqaq, R. Masana, A. Erturk and D. Dane Quinn. 'On the role of nonlinearities in vibratory energy harvesting: a critical review and discussion'. In: *Applied Mechanics Reviews* 66.4 (2014), p. 040801. DOI: 10.1115/1.4026278.

[60] S. S. Tomar and M. Talha. 'Influence of material uncertainties on vibration and bending behaviour of skewed sandwich FGM plates'. In: *Composites Part B: Engineering* 163 (2019), pp. 779–793. ISSN: 1359-8368. DOI: 10.1016/j.compositesb.2019.01.035.

[61] H. Benaroya, M. Nagurka and S. Han. *Mechanical vibration: analysis, uncertainties, and control*. CRC Press, 2017.

[62] X. Zou and A. A. Seshia. 'The impact of damping on the frequency stability of nonlinear MEMS oscillators'. In: *Journal of Microelectromechanical Systems* 24.3 (2015), pp. 537–544. DOI: 10.1109/JMEMS.2015.2391832.

[63] S. Wang, L. C. Popa and D. Weinstein. 'Piezoelectric nonlinearity in GaN Lamb mode resonators'. In: *2015 Transducers-2015 18th International Conference on Solid-State Sensors, Actuators and Microsystems (TRANSDUCERS)*. IEEE. 2015, pp. 989–992. DOI: 10.1109/TRANSDUCERS.2015.7181091.

[64] J. Zhang, Y. Wang, V. Zega, Y. Su and A. Corigliano. 'Nonlinear dynamics under varying temperature conditions of the resonating beams of a differential resonant accelerometer'. In: *Journal of Micromechanics and Microengineering* 28.7 (2018), p. 075004. DOI: 10.1088/1361-6439/aab7c6.

[65] L. Chang-Jiang, Z. Zhou-Lian, H. Xiao-Ting, S. Jun-Yi, S. Wei-Ju, X. Yun-Ping and L. Jun. 'LP perturbation solution of nonlinear free vibration of prestressed orthotropic membrane in large amplitude'. In: *Mathematical Problems in Engineering* 2010 (2010). DOI: 10.1155/2010/561364.

[66] M. Defoort, S. Hentz, S. W. Shaw and O. Shoshani. 'Amplitude stabilization in a synchronized nonlinear nanomechanical oscillator'. In: *Communications Physics* 5.1 (2022), p. 93. DOI: 10.1038/s42005-022-00861-y.

[67] I. Kozinsky, H. C. Postma, I. Bargatin and M. Roukes. 'Tuning nonlinearity, dynamic range, and frequency of nanomechanical resonators'. In: *Applied Physics Letters* 88.25 (2006), p. 253101. DOI: 10.1063/1.2209211.

[68] L. Xie, S. Baguet, B. Prabel and R. Dufour. 'Bifurcation tracking by Harmonic Balance Method for performance tuning of nonlinear dynamical systems'. In: *Mechanical Systems and Signal Processing* 88 (2017), pp. 445–461. DOI: 10.1016/j.ymssp.2016.09.037.

[69] C.-C. Yang and C.-L. Lin. 'Adaptive sliding mode control for chaotic synchronization of oscillator with input nonlinearity'. In: *Journal of Vibration and Control* 21.3 (2015), pp. 601–610. DOI: 10.1177/1077546313487243.

[70] H. Hong, C. Wu, Z. Zhao, Y. Zuo, J. Wang, C. Liu, J. Zhang, F. Wang, J. Feng, H. Shen *et al.* 'Giant enhancement of optical nonlinearity in two-dimensional materials by multiphoton-excitation resonance energy transfer from quantum dots'. In: *Nature Photonics* 15.7 (2021), pp. 510–515. DOI: 10.1038/s41566-021-00801-2.

[71] A. R. Yildiz, H. Abderazek and S. Mirjalili. 'A comparative study of recent non-traditional methods for mechanical design optimization'. In: *Archives of Computational Methods in Engineering* 27 (2020), pp. 1031–1048. DOI: 10.1007/s11831-019-09343-x.

[72] S. He, E. Prempain and Q. Wu. 'An improved particle swarm optimizer for mechanical design optimization problems'. In: *Engineering optimization* 36.5 (2004), pp. 585–605. DOI: 10.1080/03052150410001704854.

[73] Y. Starosvetsky and O. Gendelman. 'Attractors of harmonically forced linear oscillator with attached nonlinear energy sink. II: optimization of a nonlinear vibration absorber'. In: *Nonlinear Dynamics* 51 (2008), pp. 47–57. DOI: 10.1007/s11071-006-9168-z.

[74] J. R. Martins and A. Ning. *Engineering design optimization*. Cambridge University Press, 2021.

[75] M. Kegl, B. Butinar and B. Kegl. 'An efficient gradient-based optimization algorithm for mechanical systems'. In: *Communications in numerical methods in engineering* 18.5 (2002), pp. 363–371. DOI: 10.1002/cnm.499.

[76] I. Ahmadianfar, O. Bozorg-Haddad and X. Chu. 'Gradient-based optimizer: A new metaheuristic optimization algorithm'. In: *Information Sciences* 540 (2020), pp. 131–159. DOI: 10.1016/j.ins.2020.06.037.

[77] O. Dababneh, T. Kipouros and J. F. Whidborne. 'Application of an efficient gradient-based optimization strategy for aircraft wing structures'. In: *Aerospace* 5.1 (2018), p. 3. DOI: doi.org/10.3390/aerospace5010003.

[78] A. O. Pugachev. 'Application of gradient-based optimization methods for a rotor system with static stress, natural frequency, and harmonic response constraints'. In: *Structural and Multidisciplinary Optimization* 47 (2013), pp. 951–962. DOI: 10.1007/s00158-012-0867-4.

[79] S. Dou, B. S. Strachan, S. W. Shaw and J. S. Jensen. 'Structural optimization for nonlinear dynamic response'. In: *Philosophical Transactions of the Royal Society A: Mathematical, Physical and Engineering Sciences* 373.2051 (2015), p. 20140408. DOI: 10.1098/rsta.2014.0408.

[80] T. Vietor. 'Stochastic optimization for mechanical structures'. In: *Mathematical methods of operations research* 46.3 (1997), pp. 377–408. DOI: 10.1007/BF01194862.

[81] P. H. da Silva Palhares and L. da Cunha Brito. 'Stochastic optimization method for mechanical design of overhead distribution power lines'. In: *Engineering Optimization* (2019). DOI: 10.1080/0305215X.2019.1581183.

[82] A. E. Babalola, B. A. Ojokoh and J. B. Odili. 'A review of population-based optimization algorithms'. In: *2020 International Conference in Mathematics, Computer Engineering and Computer Science (ICMCECS)*. IEEE. 2020, pp. 1–7. DOI: 10.1109/ICMCECS47690.2020.240856.

[83] A. R. Kashani, C. V. Camp, M. Rostamian, K. Azizi and A. H. Gandomi. 'Population-based optimization in structural engineering: a review'. In: *Artificial Intelligence Review* (2022), pp. 1–108. DOI: 10.1007/s10462-021-10036-w.

[84] M. N. A. Wahab, S. Nefti-Meziani and A. Atyabi. 'A comprehensive review of swarm optimization algorithms'. In: *PLoS One* 10.5 (2015), pp. 1–36. DOI: 10.1371/journal.pone.0122827.

[85] D. D'Ambrosio, W. Spataro, R. Rongo, G. Iovine *et al.* 'Genetic algorithms, optimization, and evolutionary modeling'. In: *Treatise on Geomorphology-Quantitative Modeling of Geomorphology*. Vol. 2. Academic Press, 2013, pp. 74–97. DOI: 10.1371/journal.pone.0122827.

[86] B. Vahidi and A. Foroughi Nematolahi. 'Physical and physic-chemical based optimization methods: a review'. In: *Journal of Soft Computing in Civil Engineering* 3.4 (2019), pp. 12–27. DOI: 10.22115/SCCE.2020.214959.1161.

[87] H. Su, D. Zhao, A. A. Heidari, L. Liu, X. Zhang, M. Mafarja and H. Chen. 'RIME: A physics-based optimization'. In: *Neurocomputing* 532 (2023), pp. 183–214. DOI: 10.1016/j.neucom.2023.02.010.

[88] M. S. Wasim, M. Amjad, S. Habib, M. A. Abbasi, A. R. Bhatti and S. Muyeen. 'A critical review and performance comparisons of swarm-based optimization algorithms in maximum power point tracking of photovoltaic systems under partial shading conditions'. In: *Energy Reports* 8 (2022), pp. 4871–4898. DOI: 10.1016/j.egyr.2022.03.175.

[89] A. G. Gad. 'Particle swarm optimization algorithm and its applications: a systematic review'. In: *Archives of computational methods in engineering* 29.5 (2022), pp. 2531–2561. DOI: 10.1007/s11831-021-09694-4.

[90] J. Chen, B. Xin, Z. Peng, L. Dou and J. Zhang. 'Optimal contraction theorem for exploration–exploitation tradeoff in search and optimization'. In: *IEEE Transactions on Systems, Man, and Cybernetics-Part A: Systems and Humans* 39.3 (2009), pp. 680–691. DOI: 10.1109/TSMCA.2009.2012436.

[91] M. repinek, S.-H. Liu and M. Mernik. 'Exploration and exploitation in evolutionary algorithms: A survey'. In: *ACM computing surveys (CSUR)* 45.3 (2013), pp. 1–33. DOI: 10.1145/2480741.2480752.

[92] Y. Yue, L. Feng and P. Benner. 'Interpolation of reduced-order models based on modal analysis'. In: *2018 IEEE MTT-S International Conference on Numerical Electromagnetic and Multiphysics Modeling and Optimization (NEMO)*. IEEE. 2018, pp. 1–4. DOI: 10.1109/NEMO.2018.8503114.

[93] S. W. Shaw and C. Pierre. 'Modal Analysis-Based Reduced-Order Models for Nonlinear Structures— An Invariant Manifold Approach'. In: *The shock and vibration digest* 31.1 (1999), pp. 3–16. DOI: 10.1177/058310249903100101.

[94] A. H. Nayfeh and D. T. Mook. *Nonlinear oscillations*. John Wiley & Sons, 2008.

[95] A. Abolfathi, M. J. Brennan and T. P. Waters. 'Large deflection of a simply supported beam'. In: (2010).

[96] D. Midtvedt, A. Croy, A. Isacsson, Z. Qi and H. S. Park. 'Fermi-pasta-ulam physics with nanomechanical graphene resonators: intrinsic relaxation and thermalization from flexural mode coupling'. In: *Physical review letters* 112.14 (2014), p. 145503. DOI: 10.1103/PhysRevLett.112.145503.

[97] C. Touzé, O. Thomas and A. Chaigne. 'Asymmetric non-linear forced vibrations of free-edge circular plates. Part 1: Theory'. In: *Journal of Sound and Vibration* 258.4 (2002), pp. 649–676. DOI: 10.1006/jsvi.2002.5143.

[98] M. Okereke, S. Keates, M. Okereke and S. Keates. 'Direct stiffness method'. In: *Finite Element Applications: A Practical Guide to the FEM Process* (2018), pp. 47–106. DOI: 10.1007/978-3-319-67125-3_3.

[99] Y. Cheung and C. Wanji. 'Refined nine-parameter triangular thin plate bending element by using refined direct stiffness method'. In: *International Journal for Numerical Methods in Engineering* 38.2 (1995), pp. 283–298. DOI: 10.1002/nme.1620380208.

[100] R. Craig Jr. 'Substructure methods in vibration'. In: (1995). DOI: 10.1115/1.2838665.

[101] A. Y. T. Leung. 'A simple dynamic substructure method'. In: *Earthquake engineering & structural dynamics* 16.6 (1988), pp. 827–837. DOI: 10.1002/eqe.4290160605.

[102] V. Boss. 'Nonlinear dynamics of graphene membranes; Quality factor limits of membranes caused by mode interaction'. In: (). DOI: http://resolver.tudelft.nl/uuid:7ddd6ce3-831c-4ae3-96b3-9dc5bb5079bd.

5

[103] A. A. Muravyov and S. A. Rizzi. 'Determination of nonlinear stiffness with application to random vibration of geometrically nonlinear structures'. In: *Computers & Structures* 81.15 (2003), pp. 1513–1523. DOI: 10.1016/S0045-7949(03)00145-7.

[104] D. Wang, D. Tan and L. Liu. 'Particle swarm optimization algorithm: an overview'. In: *Soft computing* 22 (2018), pp. 387–408. DOI: 10.1007/s00500-016-2474-6.

[105] Y. Zhang, S. Wang, G. Ji *et al.* 'A comprehensive survey on particle swarm optimization algorithm and its applications'. In: *Mathematical problems in engineering* 2015 (2015). DOI: 10.1155/2015/931256.

[106] Q. Bai. 'Analysis of particle swarm optimization algorithm'. In: *Computer and information science* 3.1 (2010), p. 180.

[107] J. C. Bansal, P. Singh, M. Saraswat, A. Verma, S. S. Jadon and A. Abraham. 'Inertia weight strategies in particle swarm optimization'. In: *2011 Third world congress on nature and biologically inspired computing*. IEEE. 2011, pp. 633–640. DOI: 10.1109/NaBIC.2011.6089659.

[108] M. Juneja and S. Nagar. 'Particle swarm optimization algorithm and its parameters: A review'. In: *2016 International Conference on Control, Computing, Communication and Materials (ICCCCM)*. IEEE. 2016, pp. 1–5. DOI: 10.1109/ICCCCM.2016.7918233.

[109] H. Wu, C. Nie, F.-C. Kuo, H. Leung and C. J. Colbourn. 'A discrete particle swarm optimization for covering array generation'. In: *IEEE Transactions on Evolutionary Computation* 19.4 (2014), pp. 575–591. DOI: 10.1109/TEVC.2014.2362532..

[110] A. Rezaee Jordehi and J. Jasni. 'Particle swarm optimisation for discrete optimisation problems: a review'. In: *Artificial Intelligence Review* 43 (2015), pp. 243–258. DOI: 10.1007/s10462-012-9373-8.

[111] K. E. Parsopoulos, M. N. Vrahatis *et al.* 'Particle swarm optimization method for constrained optimization problems'. In: *Intelligent technologies–theory and application: New trends in intelligent technologies* 76.1 (2002), pp. 214–220.

[112] S. Kitayama, M. Arakawa and K. Yamazaki. 'Penalty function approach for the mixed discrete nonlinear problems by particle swarm optimization'. In: *Structural and Multidisciplinary Optimization* 32 (2006), pp. 191–202. DOI: 10.1007/s00158-006-0021-2.

A

PSO-STEP Integration Framework

An intricate flowchart elucidating the interaction between the PSO algorithm and the STEP method is depicted in Figure A.1. This meticulous procedure encompasses the initialization of PSO variables, the generation of various configurations, the subsequent computation of nonlinear stiffness for each configuration, and the final identification of the optimal solution upon meeting all necessary criteria.

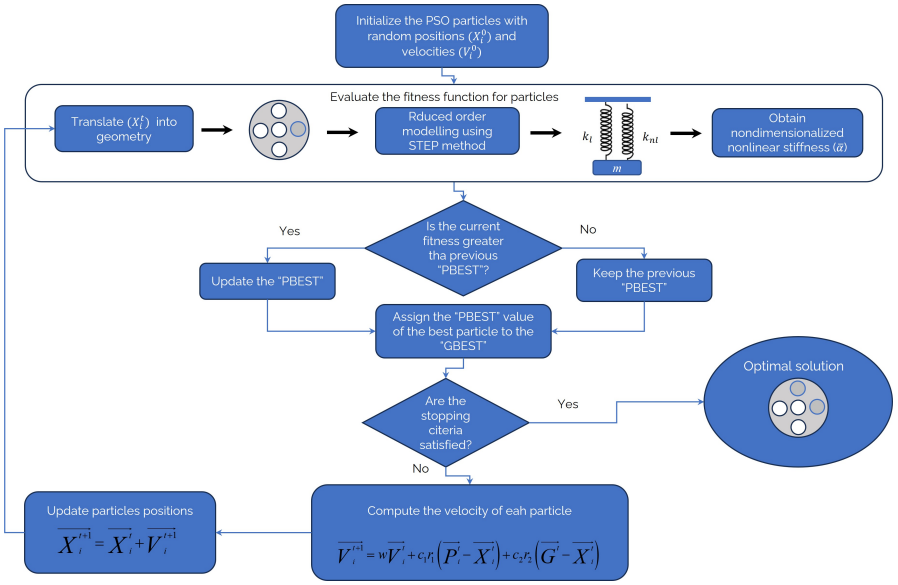

Figure A.1.: The depicted flowchart illustrates the integrated PSO-STEP algorithm, covering the initiation of PSO variables, the generation of diverse configurations, the subsequent computation of nonlinear stiffness for each configuration, and ultimately, the identification of the optimal solution upon fulfilling all specified requirements.

To comprehend the intricacies outlined in the presented flowchart (see Figure A.1), the steps can be broken down into a sequential narrative. Initially, the PSO variables are initialized in accordance with the specifics of the problem, encompassing the number of variables involved. The PSO algorithm assigns random velocity and location to each particle, facilitating an exploration of the design space. In other words, N distinct geometries are generated using these initialized PSO variables.

Following the generation of distinct geometries, the algorithm proceeds to employ the STEP method to compute the nonlinear stiffness for each initial configuration. This computation results in a vector representing the calculated stiffness values. At this stage, the algorithm seeks to assign the best PBEST value found thus far as the GBEST for the entire swarm, updating both PBEST and GBEST in each iteration.

If the stopping criteria are satisfied, signifying the attainment of the final optimal design, it is presented. However, if the optimal design remains elusive, the algorithm reverts to the PSO stage. The decision to terminate this iterative process may depend on factors such as the number of particles, iteration count, or adherence to specific constraints. This adaptive termination criterion ensures a dynamic and effective exploration of the design space.

In more detail, when the stop criteria are not satisfied, the PSO algorithm proceeds to assign new velocity and new locations to each particle (as expressed in Equation Equation (3.12) and Equation (3.13)). This results in the generation of another set of configurations. Subsequently, these newly generated configurations undergo the STEP method once again to calculate the nonlinear stiffness for each configuration.

B

NORMALIZATION PROCESS

The equation, which describes the dynamic behavior of a system subjected to a combination of linear and cubic spring forces, damping, and an external harmonic force, can be written as follows:

$$m\ddot{x} + c\dot{x} + k_l x + k_{nl} x^3 = F_e \cos(\omega t) \tag{B.1}$$

Here, m represents the mass of the system, and x is the displacement. $\ddot{x}$ and $\dot{x}$ represent the second and first derivatives of the displacement with respect to time t, respectively. c represents the damping coefficient and k_1 is the stiffness coefficient of the linear spring. The term $k_3 x^3$ denotes the cubic nonlinearity in the spring force. Additionally, $F_e \cos(\omega t)$ represents an external force applied to the system, where F_e is the amplitude of the external force, ω is the angular frequency.

Assume:

$$\hat{x} = \frac{x}{h}, \quad \tau = \omega_n t \tag{B.2}$$

$\hat{x} = \frac{x}{h}$ is defining a non-dimensional variable $\hat{x}$, which is obtained by dividing the thickness variable h. And $\tau = \omega_n t$ defines a non-dimensional time variable, where ω_n is the natural frequency of the system and t is the time variable.

The first and second derivatives of displacement with respect to time can be written as follows:

$$\frac{dx}{dt} = \frac{dh\hat{x}}{d\frac{\tau}{\omega_n}} = \frac{h\omega_n d\hat{x}}{d\tau} \tag{B.3}$$

$$\frac{d^2x}{dt^2} = \frac{d^2h\hat{x}}{d\left(\frac{\tau}{\omega_n}\right)^2} = \frac{h\omega_n^2 d^2\hat{x}}{d\tau^2} \tag{B.4}$$

By substituting Equation (B.3) and Equation (B.4) into Equation (B.1):

$$\frac{d^2\hat{x}}{d\tau^2} + \frac{c}{m\omega_n}\frac{d\hat{x}}{d\tau} + \frac{k_l}{\omega_n^2 m}x + \frac{k_{nl}h^2}{\omega_n^2 m}x^3 = \frac{F_e}{h\omega_n^2 m}\cos(\frac{\omega}{\omega_n}\tau) \tag{B.5}$$

Now, the following nondimensional variables can be introduced:

$$\begin{aligned} \zeta &= \frac{c}{2m\omega_n}, \quad \omega_n^2 = \frac{k_l}{m}, \quad \overline{k_{nl}} = \frac{k_{nl}h^2}{k_l} \\ \Omega &= \frac{\omega}{\omega_n}, \quad \hat{x}'' = \frac{\ddot{x}}{\omega_n^2 h}, \quad \hat{x}' = \frac{\dot{x}}{\omega_n h}, \quad q = \frac{F_e}{h\omega_n^2 m} \end{aligned} \tag{B.6}$$

then

$$\hat{x}'' + 2\zeta\hat{x}' + \hat{x} + \overline{k_{nl}}\hat{x}^3 = q\cos(\Omega\tau) \tag{B.7}$$

is the nondimensional form of the Equation (B.1).

C

Detailed PSO Algorithms Results

For a comprehensive understanding of the specific values and configurations discovered by each particle throughout the iterations, detailed information has been supplied in this appendix.

In Table C.1, the detailed values found by each particle in the BPSO algorithm (refer to Figure 4.9) for three different iterations are presented. It should be noted that the values are sorted from maximum to minimum values of nonlinear stiffness.

Table C.1.: Nonlinear stiffness obtained by each particle in BPSO algortihm for iterations 1, 37, and 40 (Sorted from maximum to minimum value of nonlinear stiffness).

Iteration 1	Iteration 37	Iteration 40
0.919753238	0.926796667	0.911414922
0.898916228	0.918470537	0.907991926
0.898383896	0.916288276	0.902764555
0.896844808	0.910248161	0.8990957
0.895142745	0.908814676	0.895830547
0.891884618	0.904079615	0.889891805
0.888058813	0.901254008	0.889636047
0.88670952	0.898109765	0.88959193
0.884841831	0.893943909	0.889285961
0.881929266	0.892107454	0.888402181
0.881564731	0.887582314	0.884888333
0.880580593	0.885377559	0.882857029
0.879634395	0.884115112	0.879711103
0.878839208	0.883476867	0.87909087
0.878011703	0.87662679	0.878920891
0.877765366	0.87278612	0.876073072
0.877241631	0.872187961	0.867976132
0.874634024	0.868551985	0.865010552
0.871979857	0.865443758	0.861398707
0.870945329	0.864486791	0.859589597
0.868008882	0.864126737	0.858877741
0.867343872	0.858854448	0.857447032
0.866714445	0.857204279	0.854960091
0.865046924	0.854498356	0.853958076
0.858908156	0.851346978	0.841275212
0.85704824	0.84780668	0.840776444
0.85272676	0.839411349	0.827629749
0.851326546	0.826960024	0.826924984
0.847653472	0.822677889	0.821675655
0.834346292	0.806507658	0.798986654

In Table C.2, you can find the intricate values discovered by individual particles in the DPSO algorithm (as illustrated in Figure 4.12) for three distinct iterations. It's important to mention that these values have been arranged in descending order, from the maximum to the minimum values of nonlinear stiffness.

Table C.2.: Nonlinear stiffness obtained by each particle in the DPSO algorithmfor iterations 1, 11, and 12 (Sorted from maximum to minimum values of nonlinear stiffness).

Iteration 1	Iteration 11	Iteration 12
1.02214573	1.020612183	0.960013448
0.981156946	0.997804916	0.959918896
0.945252312	0.959855761	0.946417392
0.930273977	0.949591828	0.940792115
0.928049512	0.933474063	0.934045387
0.923651346	0.92021294	0.930557147
0.921719662	0.914353676	0.922329003
0.920653499	0.902694726	0.91856678
0.91702788	0.900907386	0.916287466
0.913980445	0.898288704	0.913312758
0.913093668	0.893969937	0.910438485
0.906904777	0.888964108	0.905025935
0.900416151	0.887526202	0.8878465
0.895127245	0.881152639	0.886838565
0.894658183	0.878841774	0.881347126
0.892701053	0.876447934	0.881330942
0.89194369	0.875297448	0.878209793
0.89190208	0.87492833	0.876223354
0.888189067	0.874091104	0.872243551
0.884371689	0.873978175	0.85942031
0.882784746	0.864138284	0.850797404
0.874823549	0.857602975	0.850003047
0.874371962	0.856665405	0.841936401
0.873750487	0.853165051	0.841532695
0.857195878	0.850889685	0.837175022
0.85283311	0.839964553	0.836776013
0.834910791	0.831319656	0.829343528
0.820741234	0.827820076	0.817833477
0.802547408	0.805829397	0.814270152
0.778510415	0.778038847	0.761092417

In Table C.3, you can find the intricate values discovered by individual particles in the PSO algorithm (as illustrated in Figure 4.15) for three distinct iterations. It's important to mention that these values have been arranged in descending order, from the maximum to the minimum values of nonlinear stiffness.

Table C.3.: Nonlinear stiffness obtained by each particle for iterations 1, 25, and 29 (Sorted from maximum to minimum values of nonlinear stiffness).

Iteration 1	Iteration 25	Iteration 29
1.212201763	1.060808336	1.318749431
1.187741745	1.060525733	1.234650637
0.996113527	1.039610717	1.123624011
0.995944128	1.001214147	0.999340115
0.979966324	0.991731458	0.97638418
0.978881464	0.987382295	0.975636687
0.978634707	0.984399654	0.974690042
0.965584047	0.979677051	0.973555001
0.964137496	0.968044265	0.954026744
0.911089656	0.963391743	0.941950043
0.880927443	0.961420822	0.933365102
0.86572717	0.937676151	0.929903455
0.741849416	0.935681953	0.834828191
0.710559696	0.898797955	0.822388236
0.683325944	0.898601506	0.784136887
0.563307442	0.89838328	0.778185333
0.532240132	0.866488796	0.763806696
0.513714081	0.821839081	0.723129621
0.501296215	0.787576023	0.677708148
0.452892033	0.784328985	0.550694693
0.447274608	0.74961679	0.528845417
0.42582857	0.714492211	0.507402266
0.425501036	0.659904073	0.458821122
0.416135703	0.6135286	0.443280472
0.409068329	0.573138815	0.411036627
0.38633872	0.422790143	0.404121191
0.381683623	0.383304573	0.402847684
0.363188751	0.374040179	0.391154318
0.353666909	0.361753186	0.385967044
0.35315342	0.342441575	0.340469394

Table C.4 illustrates the nonlinear stiffness values acquired by each particle during the 1st iteration, along with their corresponding x-location and radius (r), as depicted in Figure 4.15.

Table C.4.: x-location and radius (r) for each particle for the 1st iteration (sorted from maximum to minimum values for nonlinear stiffness)

x [m]	r [m]	Nonlinear Stiffness
1.0939e-05	0.0015272	1.2122
0.00015867	0.0020429	1.1877
0.0075645	0.0013474	0.99611
0.0079365	0.001047	0.99594
0.0073938	0.00048868	0.97997
0.0082656	0.00016309	0.97888
0.0047624	0.00012226	0.97863
0.0064603	0.0012098	0.96558
0.0031936	0.0003375	0.96414
0.0028672	0.0008364	0.91109
0.0063402	0.0021601	0.88093
0.0061813	0.0022143	0.86573
0.00016003	0.0055007	0.74185
0.0035308	0.0022154	0.71056
0.0063647	0.0034794	0.68333
0.0056192	0.0039774	0.56331
0.0036907	0.0035711	0.53224
0.0018974	0.003678	0.51371
0.00024264	0.0064121	0.5013
0.001464	0.0048628	0.45289
0.0019846	0.004675	0.44727
0.0023783	0.004986	0.42583
0.0015345	0.0053395	0.4255
0.0021371	0.0052405	0.41614
0.0038097	0.0052954	0.40907
0.0017404	0.0060263	0.38634
0.0020258	0.0060401	0.38168
0.0026768	0.0063674	0.36319
0.0032016	0.0065568	0.35367
0.0015607	0.0069445	0.35315

In Table C.5, you can find the intricate values discovered by individual particles in the PSO algorithm (as illustrated in Figure 4.17) for three distinct iterations. It's important to mention that these values have been arranged in descending order, from the minimum to the maximum.

Table C.5.: Nonlinear stiffness obtained by each particle for iterations 1, 14, and 17 (Sorted from minimum to maximum values of nonlinear stiffness).

Iteration 1	Iteration 14	Iteration 17
0.398595618	0.378006045	0.367668836
0.429232132	0.416068933	0.375005549
0.434382003	0.483689044	0.420431290
0.473619621	0.512740304	0.497300083
0.475567992	0.555115645	0.518344181
0.486191633	0.606879758	0.559738002
0.509973799	0.655189807	0.573038057
0.595691055	0.677829934	0.6096752
0.709855817	0.704183825	0.619782572
0.742844441	0.790143965	0.680918225
0.743957398	0.803967801	0.687843923
0.772687613	0.853883909	0.862891284
0.782716457	0.896585789	0.876302801
0.819374532	0.944855792	0.885137172
0.908205431	0.94713233	0.886221019
0.913206735	0.949821046	0.914625803
0.926942269	0.95037964	0.914659572
0.965137657	0.951100448	0.921266798
0.969657437	0.961753857	0.921545321
0.971010919	0.966586248	0.937659971
0.971499722	0.969775171	0.954080728
0.972108617	0.973497529	0.966756364
0.973609999	0.976767164	0.980822366
0.976499846	0.977882521	0.981386713
0.980033501	0.980399539	0.983503365
0.980689631	0.981920175	1.000894595
0.988095021	0.988679603	1.001827458
1.002147775	0.989192203	1.061469041
1.003977548	1.004725026	1.637407101
1.325730571	1.6374	1.8133

In Table C.6, the nonlinear stiffness values obtained by each particle during the 1st iteration are presented, along with their respective x-location and radius (r), as depicted in Figure 4.17.

Table C.6.: x-location and radius (r) by each particle for the 1st iteration (sorted from minimum to maximum values for nonlinear stiffness)

x [m]	r [m]	Nonlinear Stiffness
0.0035332	0.0054692	0.3986
0.0021988	0.0049662	0.42923
0.0041686	0.0049168	0.43438
0.0011752	0.0047358	0.47362
0.0010568	0.0048425	0.47557
0.00089769	0.0049097	0.48619
0.0030709	0.003684	0.50997
0.0043865	0.0032497	0.59569
0.0053893	0.0028878	0.70986
0.0051866	0.0022154	0.71056
0.0041261	0.0021957	0.74284
0.0019056	0.0018048	0.74396
0.0056439	0.0025871	0.77269
0.0058241	0.0025987	0.78272
0.0028595	0.0014026	0.81937
0.0015345	0.0013691	0.90821
0.0018773	0.00083275	0.91321
0.0071403	0.0021944	0.92694
0.0035333	0.00045499	0.96514
0.0063483	0.0010196	0.96966
0.0059455	0.00096681	0.97101
0.0011556	0.00029627	0.9715
0.0016618	0.00020711	0.97211
0.0059207	0.00047944	0.97361
0.0064514	0.00080798	0.9765
0.0076269	0.00026778	0.98069
0.009344	0.00049977	0.9881
0.0080449	0.0013494	1.0021
0.0084532	0.0010476	1.004
3.171e-05	0.0022221	1.3257